# P and T-wave Delineation in ECG Signals Using a Bayesian Approach and a Partially Collapsed Gibbs Sampler

Chao Lin, Corinne Mailhes and Jean-Yves Tourneret

**Abstract**

Detection and delineation of P and T-waves are important parts in the analysis and interpretation of ECG signals. This report approaches this problem using Bayesian inference to represent a priori relationships among ECG wave components. Based on the recently introduced partially collapsed Gibbs sampler principle, the wave delineation and estimation are conducted simultaneously by using a Bayesian algorithm combined with a Markov chain Monte Carlo method. This method exploits the strong local dependency of ECG signals. The proposed strategy is evaluated on the annotated QT database and compared to other classical algorithms. An important property of this work is that it allows not only the detection of wave peaks and boundaries, but also the estimation of P and T waveforms for each analysis window. This can be useful for some ECG analysis that require wave morphology information.

**Index Terms**

ECG, P and T-wave delineation, hierarchical Bayesian analysis, partially collapsed Gibbs sampling, Markov chain Monte Carlo method.

## I. Introduction

The analysis of electrocardiograms (ECGs) has received increasing attention because of its vital role in many cardiac disease diagnosis. Most of the clinically useful information in ECGs can be found in the intervals, amplitudes or wave morphology. Therefore, the development of efficient and robust methods for automatic ECG delineation is a subject of major importance.

C. Lin, C. Mailhes and J.-Y. Tourneret are with University of Toulouse, IRIT/INP-ENSEEIHT/TéSA, 2 rue Charles Camichel, BP 7122, 31071 Toulouse cedex 7, France (e-mail:Chao.Lin@tesa.prd.fr; {Corinne.Mailhes,Jean-Yves.Tourneret}@enseeiht.fr).

The QRS complex is the most characteristic waveform of the ECG signal. Its high amplitude makes QRS detection easier than other waves. Thus, it is generally used as a reference within the cardiac cycle. Concerning P and T-wave detection and delineation (determination of peaks and limits of the individual P and T waves), algorithms usually begin with a QRS detection. Temporal search windows are then defined before and after the QRS location to seek for the other waves. Finally, an appropriate strategy is used to enhance the characteristic feature of each wave in order to find the wave peaks and boundaries.

One can find in the literature many different P and T-wave delineation approaches [1]–[20]. A first class of algorithms is based on filtering techniques, such as adaptive filters [1], low-pass differentiation (LPD) [2] and nested median filtering [3]. A second class of methods applies a basis expansion technique to the ECG signal and use the resulting coefficients for detecting P and T-waves. The different basis functions that have been considered in the literature include discrete Fourier transform [4], discrete cosine transform [5] and wavelet transform (WT) [6]–[8]. A third class of approaches considers classification and pattern recognition methods such as fuzzy theory [9], artificial neural networks [10], pattern grammars [11] and hidden Markov models [12]. Delineation can also be based upon the concept of fitting a realistic model to the ECG and extracting parameters from the model to determine waveform onsets and offsets. A particular attention has been devoted to Gaussian mixture models whose parameters can be estimated with nonlinear gradient descent [13] or Kalman filters (KF) [14], [15]. Finally, we would like to mention other delineation strategies based on length transformation [16], uniform thresholding [17], approximating function theory [18] and characterization of TU complexes [19]. Note that some of these methods can only be used to obtain a subset of P and T-wave characteristic points. Due to the low slope and low magnitude of P and T-waves and the lack of universally acknowledged clear rule to locate the beginning and the end of wave components, P and T-wave delineation remains a complicated task. Furthermore, in addition to the estimation of wave peaks and limits, an accurate waveform estimation is certainly relevant for some medical diagnoses (such as T-wave Alternans (TWA) detection [21], [22]) or pathology analysis (such as arrhythmia detection [20]).

In this report, we introduce a novel hierarchical Bayesian model which simultaneously solves the P and T-wave delineation task and the pointwise waveform estimation problems. This model takes into account appropriate prior distributions for the unknown parameters (wave locations and amplitudes, waveform coefficients). The prior distributions and the likelihood of the observed data are combined to provide the posterior distribution of the

unknown parameters. This posterior distribution depends on hyperparameters that can be fixed a priori or estimated from the observed data. This report will consider both approaches depending on the available information regarding these hyperparameters. To alleviate numerical problems related to the posterior associated to the P and T-wave delineation, we propose to resort to Markov chain Monte-Carlo (MCMC) methods [23]. MCMC are powerful sampling strategies, appropriate to solve complex Bayesian inference problems. This report concentrates on a particular MCMC method referred to as partially collapsed Gibbs sampler (PCGS) whose convergence properties have been studied in [24]. The PCGS has shown interesting properties for electromyography (EMG) [25] and optical coherence tomography (OCT) [26], [27]. However, to our knowledge, it is the first time a PCGS is applied for P and T-wave delineation in ECG signals. The ECG state sequence obeys the Markov property, since the current state (P-wave, QRS complex and T-wave) only depends on its previous state. This property inspires us to study a PCGS imposing a strong local dependency on the wave locations. This local dependency improves the convergence behavior and the computational efficiency of the sampler.

The report is organized as follows. The ECG preprocessing considered in this work is presented in Section II. Section III describes the different elements of the hierarchical Bayesian model that will be used to solve the P and T-wave delineation problems. Section IV studies a Gibbs sampler that generates samples distributed according to the posterior of the proposed hierarchical Bayesian model. The generated samples will be used to estimate the unknown model parameters and hyperparameters. The wave detection and delineation criteria based on the posterior distributions are also presented. Simulation results performed on the standard annotated QT database [28] as well as a comparison to other algorithms are given in Section V. Finally, conclusions are reported in Section VI.

## II. Preprocessing

It is common to view ECGs as the union of two parts, namely, QRS-complexes and non-QRS regions. The interval between each successive pair of QRS-offset and the subsequent QRS-onset constitutes a non-QRS region. Due to the nonstationary nature of ECGs, detection and estimation must involve a limited set of consecutive beats. In the proposed method, we first detect QRS-complexes that are the most prominent parts of the ECG signal, and we shift a nonoverlapping $D$-beat processing window to cover the whole signal. In the processing window, detected QRS-complexes become a reference for detecting P and T-waves. We define

a T search region and a P search region for each beat, relative to the QRS complex boundaries depending on a recursively computed RR interval. The T-search regions and P-search regions within the processing window are then extracted individually to form a T-wave search block and a P-wave search block. The preprocessing procedure can be summarized as follows:

*1) QRS detection:* QRS complexes are detected using Pan $et\ al.$'s algorithm [29] based on digital analysis of slope, amplitude and width. The filtering that is done prior to this algorithm is found to be satisfactory. Thus no additional filtering is required before the delineation of P and T-waves. Note however that any other QRS detection algorithm could be used in this preprocessing step.

*2) Removal of baseline drift:* In the proposed algorithm, waveform coefficients are estimated simultaneously with the wave detection. Baseline drift causes inaccurate waveform estimation results. For this reason, we employ the method proposed in [30] to remove baseline drift in each RR interval.

*3) Construction of P and T-wave search blocks:* As shown in Fig. 1, in the $D$-beat processing window, $D$ successive right-hand neighborhoods of QRS offsets can be extracted to form a T-wave search block. Similarly, $D$ left-hand neighborhoods of QRS onsets can be extracted to form a P-wave search block. Suppose that $k_{\text{off}}$ denotes a QRS offset location, then a T-wave indicator can only appear in the right-hand neighborhood of $k_{\text{off}}$ which can be denoted as $J_T(k_{\text{off}}) = (k_{\text{off}}+1, \ldots, k_{\text{off}}+N_T)$, where $N_T$ denotes the T-wave search region width. Similarly, a P-wave indicator can only appear in the left-hand neighborhood of a QRS onset location $k_{\text{on}}$. It can be denoted as $J_P(k_{\text{on}}) = (k_{\text{on}}-N_P, \ldots, k_{\text{on}}-1)$, where $N_P$ denotes the P-wave search region width. The length of each target neighborhood could be fixed either according to the cardiologists or related to the current estimated RR interval (denoted by RRI). The amount of neighborhoods in each block depends on the length of the processing window.

The proposed algorithm processes two search blocks (one for T-wave delineation and the other for P-wave delineation) individually using the same Bayesian inference. Section III introduces the Bayesian model applied to T-wave search block, while it should be noted that this model is compatible for P-wave search block as well.

## III. Hierarchical Bayesian model for T-waves

Deconvolution models have been widely used in many signal processing applications including signal segmentation [31], layer detection [26], and EMG signal analysis [32].

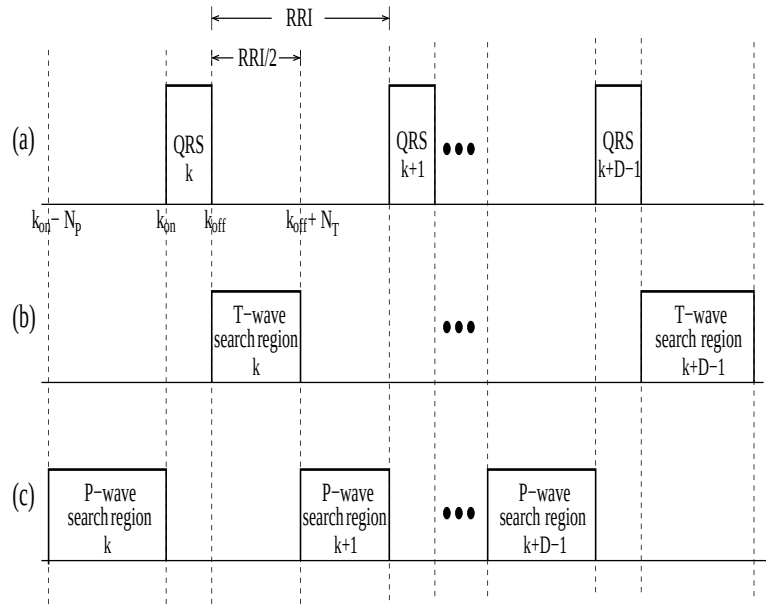


Fig. 1. Preprocessing procedure within the $D$-beat processing window: (a) Located QRS complexes. (b) T-wave searching block. (c) P-wave searching block. RRI is the interval between the present QRS offset and the next QRS onset and RRI/2 is half of RRI, here we set $N_T = N_P =$RRI/2.

Following these ideas, signals in T-wave search blocks are assumed to be the convolution of an unknown impulse response $\mathbf{h} = [h_0, \ldots, h_L]^T$ with an unknown input sequence $\mathbf{u} = [u_1, \ldots, u_M]^T$ such that

$$x_k = \sum_{l=0}^{L} h_l u_{k-l} + n_k \tag{1}$$

with $k \in \{1, \ldots, K\}$, $K = M + L$ is the block length, and $n_k$ denotes the additive Gaussian noise with variance $\sigma_n^2$. Here, we adopt a zero boundary condition, i.e., the unknown sequence $u_m$ is assumed to vanish for all $m \notin \{1, \ldots, M\}$. In matrix form, (1) can be written as

$$\mathbf{x} = \mathbf{F}\mathbf{u} + \mathbf{n} \tag{2}$$

where $\mathbf{x} = [x_1, \ldots, x_K]^T$, $\mathbf{n} = [n_1, \ldots, n_K]^T$, $\mathbf{F}$ is the Toeplitz matrix of size $K \times M$ with first row $[h_0\ \mathbf{0}_{M-1}]$ and first column $\left[\mathbf{h}^T\ \mathbf{0}_{M-1}\right]^T$ ($\mathbf{0}_{M-1}$ is a $(M-1) \times 1$ vector of zeros)

$$\mathbf{F} = \begin{bmatrix} h_0 & 0 & \cdots & 0 \\ \vdots & \ddots & \cdots & \vdots \\ h_L & h_{L-1} & \cdots & 0 \\ 0 & h_L & \ddots & \vdots \\ \vdots & \ddots & \ddots & h_{L-1} \\ 0 & \cdots & 0 & h_L \end{bmatrix}_{K \times M}.$$

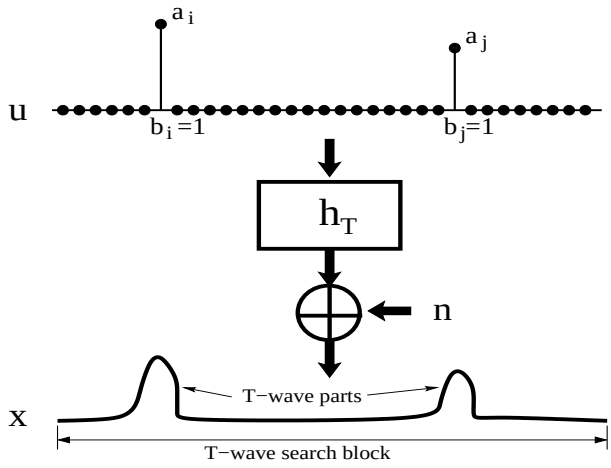


Fig. 2. Modeling of T-wave parts within the T-wave search block.

The sequence **u** can be further decomposed as a binary sequence $b_m \in \{0,1\}, m = 1,\ldots,M$ indicating the T-wave existence multiplied by weight factors $\mathbf{a} = [a_1,\ldots,a_M]^T$ representing the T-wave amplitudes, as illustrated in Fig. 2. Note that the impulse response **h** is supposed to be unique for $D$ T-wave search regions within the processing window whereas the amplitudes **a** vary from one region to another. Consequently, (2) can be written as

$$\mathbf{x} = \mathbf{FBa} + \mathbf{n} \tag{3}$$

where **B** denotes the $M \times M$ diagonal matrix diag $(\mathbf{b})$ and $\mathbf{b} = [b_1,\ldots,b_M]^T$.

The unknown parameter vector resulting from this reparameterization is $\boldsymbol{\theta} = \left[\mathbf{b}^T, \mathbf{a}^T, \mathbf{h}^T, \sigma_n^2\right]^T$. This report proposes to estimate the unknown parameter vector $\boldsymbol{\theta}$ by using Bayesian estimation theory. Bayesian inference on $\boldsymbol{\theta}$ is based on the posterior distribution $p(\boldsymbol{\theta}|\mathbf{x}) \propto p(\mathbf{x}|\boldsymbol{\theta})\, p(\boldsymbol{\theta})$ (where $\propto$ means "proportional to"), which is related to the likelihood of the observations and the parameter priors. The likelihood $p(\mathbf{x}|\boldsymbol{\theta})$ and prior $p(\boldsymbol{\theta})$ for the T-wave delineation problem are summarized below.

### *A. Likelihood*

Using (3), the likelihood of the observed data vector **x** can be expressed as

$$p\left(\mathbf{x}|\mathbf{b},\mathbf{a},\mathbf{h},\sigma_n^2\right) = \frac{1}{(2\pi)^{\frac{K}{2}}\,\sigma_n^K} \exp\left[-\frac{1}{2\sigma_n^2}\left\|\mathbf{x}-\mathbf{FBa}\right\|^2\right]$$

where $\|\mathbf{x}\| = \left(\mathbf{x}^T\mathbf{x}\right)^{\frac{1}{2}}$ denotes the Euclidean norm.

*B. Prior distributions*

We propose to model the unknown sequence $u_k = a_k b_k$ as a Bernoulli-Gaussian (BG) sequence

$$b_k \sim \mathcal{B}e(\lambda), \quad a_k|b_k = 1 \sim \mathcal{N}\left(0, \sigma_a^2\right) \tag{4}$$

where $\mathcal{B}e(\lambda)$ is the Bernoulli distribution with parameter $\lambda$ such that $p[b_k = 1] = \lambda$. In order to handle both positive and negative wave amplitudes, $a_k$ is distributed according to a zero mean Gaussian distribution with variance $\sigma_a^2$ when $b_k = 1$, whereas $a_k = 0$ otherwise.

Because of the Markov property of ECG, successive T-waves can only appear in search regions located in the right-hand neighborhoods of each QRS offset (whereas P-waves are located to the left-hand neighborhoods of each QRS onset). Thus the T-wave indicator vector $\mathbf{b}$ cannot have two elements $b_k = 1$ and $b_{k'} = 1$ closer than a minimum-distance constraint $d$, where $d$ depends on the RR interval length. Consequently, the T-wave detection problem can be seen as a BG blind deconvolution problem with deterministic local constraints as in [26], [27]. The prior of $\mathbf{b}$ can then be defined as the product of a minimum-distance constraint indicator function $I_C(\mathbf{b})$ and the likelihood of independent Bernoulli random variables

$$p(\mathbf{b}) \propto \left( \prod_{k=1,\ldots,K} p(b_k) \right) I_C(\mathbf{b})$$

where $I_C(\mathbf{b})$ enforces the minimum-distance constraint $\mathbf{b} \in C$, i.e., $I_C(\mathbf{b}) = 1$ if $\mathbf{b} \in C$ and $I_C(\mathbf{b}) = 0$ if $\mathbf{b} \notin C$.

Since there is no relation between the noise, the impulse response and the BG sequence, $\sigma_n^2$, $\mathbf{h}$ and $(\mathbf{b}, \mathbf{a})$ are assigned a priori independent priors such that $p(\boldsymbol{\theta}) = p(\mathbf{b}, \mathbf{a})\, p(\mathbf{h})\, p(\sigma_n^2)$. The impulse response $\mathbf{h}$, and noise $\mathbf{n}$ are assigned Gaussian priors: $p(\mathbf{h}) = \mathcal{N}(\mathbf{0}, \sigma_h^2 \mathbf{I}_{L+1})$, and $p(\mathbf{n}) = \mathcal{N}(\mathbf{0}, \sigma_n^2 \mathbf{I}_K)$, where $\mathbf{I}_N$ denotes the identity matrix of size $N \times N$. Choosing conjugate Gaussian priors for $\mathbf{a}$ and $\mathbf{h}$ considerably simplifies the algorithm since the resulting conditional distributions are also Gaussian. Here, $\sigma_a^2$ and $\sigma_h^2$ are fixed hyperparameters whereas the noise variance $\sigma_n^2$ is estimated jointly with the other parameters using a hierarchical Bayesian model. The impulse response is normalized to avoid scale ambiguity (different values of amplitude and impulse response could provide the same convolution results) such that $\sigma_h^2 = 1$. Moreover, the proposed algorithm normalizes the ECG signals with different amplitude resolutions by their maximum R-peak amplitude such that $\sigma_a^2 = 1$ can cover all possible amplitude values. For the prior of $\sigma_n^2$, we use an inverse gamma distribution $IG(\xi, \eta)$

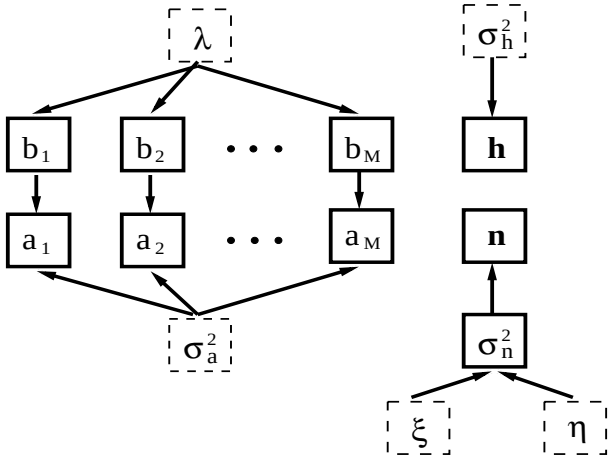


Fig. 3. DAG for the prior distributions; the fixed parameters appear as dashed boxes.

as suggested in [31], where $\xi$ and $\eta$ are fixed hyperparameters providing a vague prior (few informative).

### C. Posterior distribution

The posterior distribution of the unknown parameters can be computed from the following hierarchical structure

$$p\left(\boldsymbol{\theta}|\mathbf{x}\right) \propto p\left(\mathbf{x}|\boldsymbol{\theta}\right) p\left(\mathbf{a}|\mathbf{b}\right) p\left(\mathbf{b}\right) p\left(\mathbf{h}\right) p\left(\sigma_n^2\right). \tag{5}$$

This hierarchical structure is shown on the directed acyclic graph (DAG) of Fig. 3. The usual Bayesian estimators related to this posterior are the minimum mean square error (MMSE) estimator and the maximum a posteriori (MAP) estimators [33]. Due to the complexity of the posterior distribution (5), it is difficult to obtain closed-form expressions of these estimators. As a consequence, we propose to study an MCMC method which generates samples asymptotically distributed according to the target distribution (5). The MMSE or MAP estimators of the unknown parameters are then computed using the generated samples. The main principles of MCMC methods can be found in [23]. The Gibbs sampler (GS) used to generate samples distributed according to (5) is detailed in the next section.

## IV. Gibbs samplers for wave extraction

### A. Standard Gibbs Sampler

To obtain samples from $p\left(\mathbf{b}, \mathbf{a}, \mathbf{h}, \sigma_n^2|\mathbf{x}\right)$, the standard GS iteratively generates samples from $p\left(\mathbf{b}|\mathbf{a}, \mathbf{h}, \sigma_n^2, \mathbf{x}\right)$, $p\left(\mathbf{a}|\mathbf{b}, \mathbf{h}, \sigma_n^2, \mathbf{x}\right)$, $p\left(\mathbf{h}|\mathbf{a}, \mathbf{b}, \sigma_n^2, \mathbf{x}\right)$ and $p\left(\sigma_n^2|\mathbf{a}, \mathbf{b}, \mathbf{h}, \mathbf{x}\right)$ as summarized in

Algorithm 1.

**Algorithm 1** the classical GS

**for** $k = 1$ to K **do**

Sample $b_k$ from $p\left(b_k|\mathbf{b}_{\sim k}, \mathbf{a}, \mathbf{h}, \sigma_n^2, \mathbf{x}\right)$

**end for**

Sample $\mathbf{a}$ from $p\left(\mathbf{a}|\mathbf{b}, \mathbf{h}, \sigma_n^2, \mathbf{x}\right)$

Sample $\mathbf{h}$ from $p\left(\mathbf{h}|\mathbf{b}, \mathbf{a}, \sigma_n^2, \mathbf{x}\right)$

Sample $\sigma_n^2$ from $p\left(\sigma_n^2|\mathbf{b}, \mathbf{a}, \mathbf{h}, \mathbf{x}\right)$

Here, $\mathbf{b}_{\sim k}$ denotes the vector $\mathbf{b}$ without its $k^{\text{th}}$ component. As pointed out in [27], this classical GS is poorly suited to problems with local constraints because a constraint that excludes parts of the hypothesis space may even inhibit convergence to $p\left(\mathbf{b}, \mathbf{a}, \mathbf{h}, \sigma_n^2|\mathbf{x}\right)$ altogether.

### *B. Partially Collapsed Gibbs Sampler*

In our case, the unknown parameter vector $\boldsymbol{\theta}$ can be split into two parts, i.e., $(\mathbf{b}, \mathbf{a})$ that contains constrained parameters and $(\mathbf{h}, \sigma_n^2)$ that contains unconstrained parameters. To accelerate the convergence of the Gibbs sampler, we propose a PCGS that takes into considerations the local constraints affecting $\mathbf{b}$ and $\mathbf{a}$. More precisely, denote as $J_d\left(k\right)$ a right-hand neighborhood of $k$ with length $d$, i.e., $J_d\left(k\right) = \{k, \ldots, k+d-1\}$ and divide the wave indicator vector $\mathbf{b}$ and the wave amplitude vector $\mathbf{a}$ into two parts $\mathbf{b}_{J_d(k)} = (b_k, \ldots, b_{k+d-1})$, $\mathbf{b}_{\sim J_d(k)} = (b_1, \ldots, b_{k-1}, b_{k+d}, \ldots, b_K)$ and $\mathbf{a}_{J_d(k)} = (a_k, \ldots, a_{k+d-1})$, $\mathbf{a}_{\sim J_d(k)} = (a_1, \ldots, a_{k-1}, a_{k+d}, \ldots, a_K)$. The proposed PCGS iteratively generates $b_k$ and $a_k$ according to the conditional distributions $p\left(b_k|\mathbf{b}_{\sim J_d(k)}, \mathbf{a}_{\sim J_d(k)}, \mathbf{h}, \sigma_n^2, \mathbf{x}\right)$ and $p\left(a_k|b_k, \mathbf{b}_{\sim J_d(k)}, \mathbf{a}_{\sim J_d(k)}, \mathbf{h}, \sigma_n^2, \mathbf{x}\right)$. The resulting algorithm is summarized in Algorithm 2 whereas the different conditional distributions are derived in the appendix and detailed below. Note that the convergence of this sampler to the target distribution (5) directly results from [24] (see also [25] and [26] for applications of the PCGS).

**Indicators.** The sampling distribution for $b_k$ is a conditional distribution associated with the joint posterior $p\left(\mathbf{b}, \mathbf{a}, \mathbf{h}, \sigma_n^2|\mathbf{x}\right)$ marginalized with respect to the remaining parameters in the neighborhood $J_d\left(k\right) \setminus k = \{k+1, \ldots, k+d-1\}$. Thus, $\mathbf{b}_{J_d(k)}$ is not contained in the condition for $b_k$. The marginalization of the joint posterior is rarely possible to be done analytically with respect to $\mathbf{b}_{J_d(k)\setminus k} = [b_{k+1}, \ldots, b_{k+d-1}]^T$. Indeed, this conditional distribution can

**Algorithm 2** the proposed PCGS

set k = 1

**while** $k \leq K$ **do**

sample $b_k$ from $p\left(b_k|\mathbf{b}_{\sim J_d(k)}, \mathbf{a}_{\sim J_d(k)}, \mathbf{h}, \sigma_n^2, \mathbf{x}\right)$

**if** $b_k = 1$ **then**

sample $a_k$ from $p\left(a_k|b_k = 1, \mathbf{b}_{\sim J_d(k)}, \mathbf{a}_{\sim J_d(k)}, \mathbf{h}, \sigma_n^2, \mathbf{x}\right)$

set $\mathbf{b}_{J_d(k)\setminus k} = \mathbf{0}$

set $k = k + d - 1$

**end if**

set $k = k + 1$

**end while**

sample $\mathbf{h}$ from $p\left(\mathbf{h}|\mathbf{b}, \mathbf{a}, \sigma_n^2, \mathbf{x}\right)$

sample $\sigma_n^2$ from $p\left(\sigma_n^2|\mathbf{b}, \mathbf{a}, \mathbf{h}, \mathbf{x}\right)$

be calculated as $p\left(b_k|\mathbf{b}_{\sim J_d(k)}, \mathbf{a}_{\sim J_d(k)}, \mathbf{h}, \sigma_n^2, \mathbf{x}\right) = \sum_{\mathbf{b}_{J_d(k)\setminus k}} p\left(\mathbf{b}_{J_d(k)}|\mathbf{b}_{\sim J_d(k)}, \mathbf{a}_{\sim J_d(k)}, \mathbf{h}, \sigma_n^2, \mathbf{x}\right)$. Thus, we propose to sample $\mathbf{b}_{J_d(k)}$ from $p\left(\mathbf{b}_{J_d(k)}|\mathbf{b}_{\sim J_d(k)}, \mathbf{a}_{\sim J_d(k)}, \mathbf{h}, \sigma_n^2, \mathbf{x}\right)$ and then use the $b_k$ contained in the sample. Therefore, the sampling distribution for wave indicators is

$$p\left(\mathbf{b}_{J_d(k)}|\mathbf{b}_{\sim J_d(k)}, \mathbf{a}_{\sim J_d(k)}, \mathbf{h}, \sigma_n^2, \mathbf{x}\right) \propto \sigma_1 \exp\left(\frac{|\mu_1|^2}{2\sigma_1^2}\right) p\left(\mathbf{b}\right)$$

with

$$\sigma_1^2 = \left(\frac{\left\|\mathbf{F}_{J_d(k)}\mathbf{b}_{J_d(k)}\right\|^2}{\sigma_n^2} + \frac{1}{\sigma_a^2}\right)^{-1}$$

$$\mu_1 = \frac{\sigma_1^2 \mathbf{b}_{J_d(k)}^T \mathbf{F}_{J_d(k)}^T \left(\mathbf{x} - \mathbf{F}_{\sim J_d(k)}\mathbf{B}_{\sim J_d(k)}\mathbf{a}_{\sim J_d(k)}\right)}{\sigma_n^2}$$

where $\mathbf{F}_{J_d(k)}$ denotes the columns of $\mathbf{F}$ indexed by $J_d\left(k\right)$, $\mathbf{F}_{\sim J_d(k)}$ denotes $\mathbf{F}$ without those columns, and $\mathbf{B}_{\sim J_d(k)}$ denotes the diagonal matrix diag $\left(\mathbf{b}_{\sim J_d(k)}\right)$ (see appendix for computation details).

**Amplitudes.** Using the fact that $p\left(\mathbf{a}\right)$ is a conjugate prior, we obtain

$$p\left(a_k|b_k = 1, \mathbf{b}_{\sim J_d(k)}, \mathbf{a}_{\sim J_d(k)}, \mathbf{h}, \sigma_n^2, \mathbf{x}\right) = \mathcal{N}\left(\mu_1, \sigma_1^2\right).$$

Note that the amplitude $a_k$ is sampled only when $b_k = 1$, i.e., when a wave has been detected.

**Waveform coefficients.** Because **h** is a priori Gaussian, it can be treated as one parameter in the Gibbs sampler without introducing excessive complexity. As a consequence

$$p\left(\mathbf{h}|\mathbf{b},\mathbf{a},\sigma_n^2,\mathbf{x}\right)=\mathcal{N}\left(\boldsymbol{\mu}_2,\boldsymbol{\sigma}_2^2\right)$$

with

$$\boldsymbol{\mu}_2=\frac{\boldsymbol{\sigma}_2^2\mathbf{U}^T\mathbf{x}}{\sigma_n^2},\quad \boldsymbol{\sigma}_2^2=\left(\frac{\mathbf{U}^T\mathbf{U}}{\sigma_n^2}+\frac{\mathbf{I}_{L+1}}{\sigma_h^2}\right)^{-1}$$

where **U** is the Toeplitz matrix of size $K\times(L+1)$ with first row $[u_1\ \mathbf{0}_L]$ and first column $\left[\mathbf{u}^T\ \mathbf{0}_L\right]$

$$\mathbf{U}=\begin{bmatrix} u_1 & 0 & \cdots & 0\\ \vdots & \ddots & \cdots & \vdots\\ u_M & u_{M-1} & \cdots & 0\\ 0 & u_M & \ddots & \vdots\\ \vdots & \ddots & \ddots & u_{M-1}\\ 0 & \cdots & 0 & u_M \end{bmatrix}_{K\times(L+1)}.$$

Note that **Uh** is equivalent to **FBa**, thus (3) can be represented as $\mathbf{x}=\mathbf{Uh}+\mathbf{n}$. As mentioned in III.A, scale ambiguity inherent to the convolution model can be resolved by normalizing **h** in every iteration.

**Noise variance.** As explained in [31], the conditional distribution of the noise variance is the following inverse gamma distribution

$$p\left(\sigma_n^2|\mathbf{b},\mathbf{a},\mathbf{h},\mathbf{x}\right)=IG\left(\xi+\frac{K}{2},\eta+\frac{1}{2}\left\|\mathbf{x}-\mathbf{FBa}\right\|^2\right).$$

### *C. P and T-wave detection and delineation criteria*

P and T-wave detection and delineation are based on the estimated posterior distributions of wave indicators, wave amplitudes and waveform coefficients. These estimated posteriors are computed from histograms of the samples generated by the PCGS.

*1) P and T-wave detection:* Unlike most of the approaches found in the literature, no rigid amplitude threshold is used to determine whether waves are significant or not. The posterior distribution of wave indicators carries information regarding the probability of having a P or T-wave at a given location. Thus the detection results $\hat{\mathbf{b}}$ can be obtained with various degrees of certainty by using a local maximum posterior strategy. Since there can only be one T-wave (P-wave) in each T-searching neighborhood (P-searching neighborhood), the proposed algorithm compares the highest estimated posterior probability in each neighborhood with

a given probability threshold ($\gamma_P$ for P-wave and $\gamma_T$ for T-wave) to decide whether it is significant or not. If a local maximum posterior probability is higher than the threshold, the corresponding indicator location can be seen as the estimate wave location in this searching neighborhood. Note that the estimated indicator posterior probability at position $k$ is defined as follows (the probability of having $b_k = 1$ equals $\mathrm{E}[b_k]$, where $\mathrm{E}[\bullet]$ is the mathematical expectation since $b_k$ is a binary random variable)

$$\hat{b}_{k,\mathrm{MMSE}} = \frac{1}{N_r} \sum_{t=1}^{N_r} b_k^{(N_{\mathrm{bi}}+t)} \tag{6}$$

where $b_k^{(t)}$ denotes the indicator at position $k$ generated at iteration $t$, while $N_r$ is the number of iterations and $N_{\mathrm{bi}}$ is the number of burn-in[1] iterations.

When using low values of $\gamma_T$ and $\gamma_P$ to increase detection sensitivity, this strategy can still ensure no more than one wave detection in each target neighborhood. Thus, it can avoid missing detections of T or P-waves without increasing false positives.

*2) Estimation of wave amplitudes, waveforms and noise variance:* For estimating the wave amplitudes $a_k$ corresponding to position $k$ where a P or T-wave has been detected, we use the MMSE estimator of $a_k$ conditionally upon $b_k = 1$ as shown in (7)

$$\hat{a}_{k,\mathrm{MMSE}} = \frac{1}{|\mathcal{T}_k|} \sum_{t \in \mathcal{T}_k} a_k^{(t)} \tag{7}$$

where $a_k^{(t)}$ denotes the $k^{\mathrm{th}}$ entry of the amplitude vector **a** generated by the Markov chain at iteration $t$, $\mathcal{T}_k$ is the set of indices $t$ of all iterations satisfying $b_k^{(t)} = 1$ excluding burn-in iterations. Note that $\hat{a}_{k,\mathrm{MMSE}}$ is calculated only when a P or T-wave has been detected.

Concerning the waveform coefficients **h** and noise variance $\sigma_n^2$, the MMSE estimators are given by (8) and (9)

$$\hat{\mathbf{h}}_{\mathrm{MMSE}} = \frac{1}{N_r} \sum_{t=1}^{N_r} \mathbf{h}^{(N_{\mathrm{bi}}+t)} \tag{8}$$

$$\hat{\sigma_n^2}_{\mathrm{MMSE}} = \frac{1}{N_r} \sum_{t=1}^{N_r} \left(\sigma_n^2\right)^{(N_{\mathrm{bi}}+t)} \tag{9}$$

where $\mathbf{h}^{(t)}$ and $(\sigma_n^2)^{(t)}$ denote respectively **h** and $\sigma_n^2$ generated at iteration $t$.

[1]The burn-in period corresponds to the first iterations of the sampler that are not used for estimating the unknown parameters

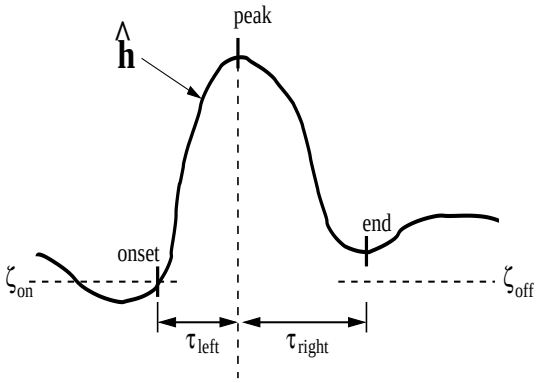


Fig. 4. Parameters of the wave delineation method.

*3) P and T-wave delineation:* Since the estimated waveform $\hat{\mathbf{h}}_{\text{MMSE}}$ carries information regarding the wave morphology, we propose a delineation criteria which is based on the waveform estimate of each processing window.

First of all, the onset and end of $\hat{\mathbf{h}}_{\text{MMSE}}$ are determined by applying two criteria: i) searching for the sample where $\hat{h}_n$ is below a threshold ($\zeta_{\text{Pon}}$ and $\zeta_{\text{Poff}}$ for P waves, $\zeta_{\text{Ton}}$ and $\zeta_{\text{Toff}}$ for T waves) proportional to the maximum modulus of $\hat{\mathbf{h}}_{\text{MMSE}}$; ii) searching for a local minimum of $\hat{\mathbf{h}}_{\text{MMSE}}$ before or after the wave peak. The samples that supply either of these two criteria are accepted as candidates. The onset of $\hat{\mathbf{h}}_{\text{MMSE}}$ is selected as the candidate that supplies the nearest sample before the peak and the end is selected as the candidate that supplies the nearest sample after the peak. Fig. 4 illustrates this definition of the onset and the end of a wave, where the onset-peak distance and the peak-end distance of $\hat{\mathbf{h}}_{\text{MMSE}}$ are denoted by $\tau_{\text{left}}$ and $\tau_{\text{right}}$, respectively. In this example, onset is the first time instant for which the estimated waveform coefficient is below the threshold $\zeta_{\text{Pon}}$. Moreover, since all values of the estimated waveform located on the right of peak are above the threshold, end has been estimated as the first local minimum on the right of this peak.

*Remark 1:* We have observed that allowing the wave length to change within a processing window can further improve delineation performance. Considering a wave within the processing window whose wave peak is located at sample $k$ (i.e., $\hat{b}_{k,\text{MMSE}} = 1$), we propose to compute its onset and end locations as follows

$$\begin{cases} \text{onset}_k = \text{round}\left(k - \eta_k \tau_{\text{left}}\right) \\ \text{end}_k = \text{round}\left(k + \eta_k \tau_{\text{right}}\right) \end{cases}$$

where $\eta_k = \frac{\hat{a}_{k,\text{MMSE}}}{\bar{\mathbf{a}}_{\text{MMSE}}}$ and $\bar{\mathbf{a}}_{\text{MMSE}}$ is the average estimated amplitude within the block. In practical

situation, $\eta_k$ will be close to 1 and not exactly equal to 1.

As there is no universally acknowledged clear rule to locate onsets and ends of waves, the delineation thresholds have been obtained by minimizing the error between estimates and published annotations. The following results have been obtained for the QT database

$$\begin{cases} \zeta_{\text{Ton}} = 0.02\text{max}\left(\hat{\mathbf{h}}_T\right) \\ \zeta_{\text{Toff}} = 0.1\text{max}\left(\hat{\mathbf{h}}_T\right) \\ \zeta_{\text{Pon}} = 0.05\text{max}\left(\hat{\mathbf{h}}_P\right) \\ \zeta_{\text{Poff}} = 0.1\text{max}\left(\hat{\mathbf{h}}_P\right) \end{cases}.$$

The general flowchart for the proposed algorithm including preprocessing, PCGS and wave delineation is shown in Fig. 5.

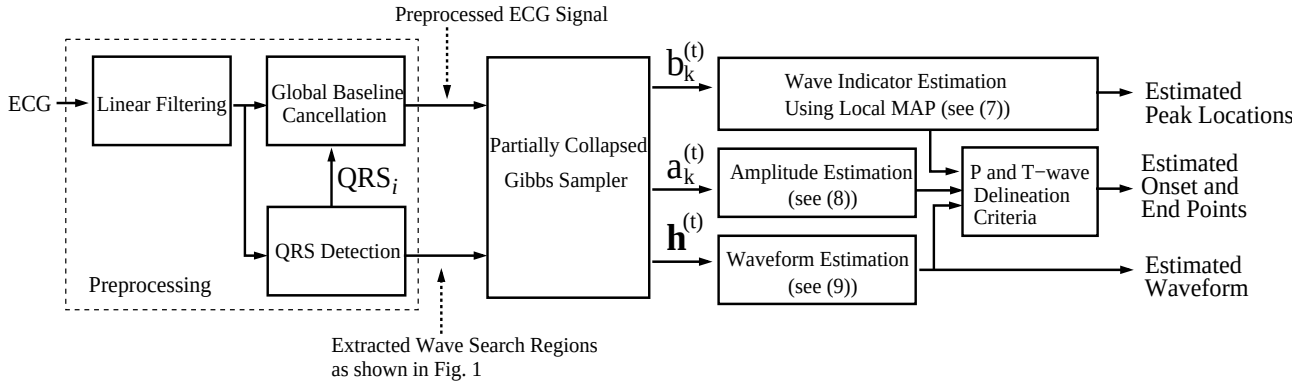


Fig. 5. General block diagram for the proposed P and T-wave delineation algorithm.

## V. Simulation results

Many simulations have been conducted to validate the algorithm proposed before. First, we show some posterior distributions and estimation results for one typical example. Then, graphical evaluations and analytical results on an entire standard database are presented. At last, a standard criterion has been used to study the convergence of the proposed PCGS. Usually, the validation of the ECG wave detector or delineator is done using manually annotated database. In this report, we use one of the easily-available standard databases, namely the QT database (QTDB) [28]. The QTDB includes some records from the widely used MIT-BIH Arrhythmia database (MITDB), the European ST-T database (EDB) and some other well known databases. This database was developed in the purpose of providing a wave limit validation reference. It provides cardiologist annotations for at least 30 beats per

recording for both channels. The cardiologist annotations include QRS complexes, P and T wave peaks, onsets and ends for at least 3600 beats (some of the annotated records contain only a subset of waveform patterns). The proposed algorithm works on a single-channel basis, while the cardiologist annotations were performed having in sight all available leads. Therefore, to compare in a reasonable way the manual annotations on the QTDB with the two signal-channel annotations produced by the proposed delineator, we choose for each point the channel with less error. The QTDB also includes an additional annotation performed by a second cardiologist. However, this annotation only exists for 11 out of 105 records. Thus it has not been considered in our study.

### *A. One typical example*

The first simulations have been obtained by applying the proposed algorithm on dataset "sele0136" of QTDB at minute 10. This example has been chosen because the signal from this data set presents some rhythm changes with different amplitudes between P and T-waves. The processing window length $D$ has been set to 8 beats, which corresponds to about 2200 samples. For each P or T-wave search block, we generated 100 realizations according to the priors given in Section III using $\sigma_a^2 = 1$, $\sigma_h^2 = 1$, $\xi = 11$ and $\eta = 0.5$ (these are fixed hyperparameters to provide a noninformative prior). The value of $\lambda$ is fixed by calculating the division of R peak numbers within the processing window and the window length $K$. We considered $N_{\text{bi}} = 40$ burn-in iterations (the way $N_{\text{bi}}$ has been adjusted is explained in Section VI.D). Thus, only the last 60 Markov chain output samples were used for computing the estimates. Note that running 100 iterations of the proposed algorithm for a 10-beat ECG block sampled at $Fs = 250$Hz (i.e., ECG signals lasting about 10 seconds) takes approximately 13 seconds for a MATLAB® implementation on a 3.0-GHz Pentium IV. However, these codes might be further optimized and converted to low-level languages for clinical use.

As mentioned before, the estimates of the unknown parameters are derived from their posterior distributions. Fig. 6 shows the posterior distributions of wave indicator locations $p(\mathbf{b}|\mathbf{x})$ estimated by using the last 60 Markov chain iterations. The posterior probability is very high for most of the actual P and T-wave locations except for P-wave indicators around time instant 4.45. Indeed, the algorithm seems hesitant to locate P-wave indicators around this location. If we employ a simple rigid threshold on the entire block, there is a chance this wave indicator will be missed in the estimation. However, with the local maximum posterior

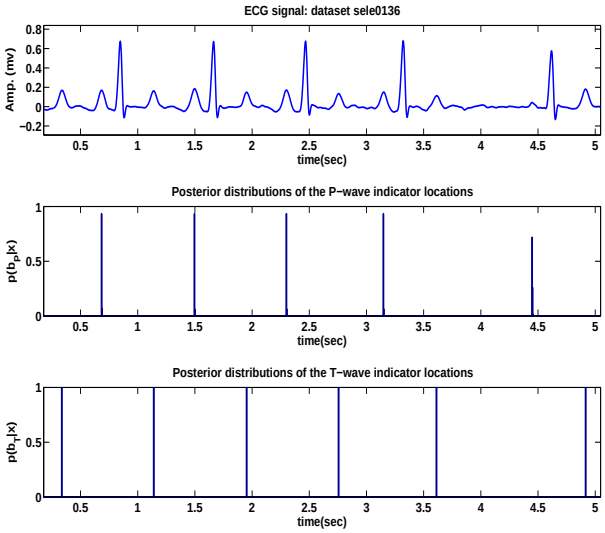


Fig. 6. Posterior distributions of the P-wave indicator locations $p\left(\mathbf{b}_{\mathrm{P}}|\mathbf{x}\right)$ (middle) and the T-wave indicator locations $p\left(\mathbf{b}_{\mathrm{T}}|\mathbf{x}\right)$ (bottom) of ECG signal part (top).

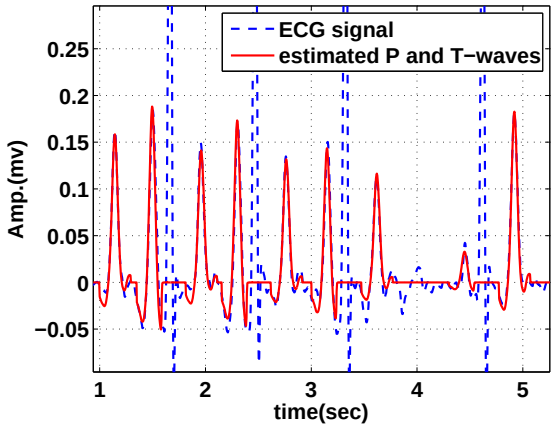


Fig. 7. Real ECG signal dataset “sele0136” (dashed blue) and estimated P and T-waves (red).

strategy explained in Section IV, a relatively low value of $\gamma_P$ can be employed to ensure the detection of low magnitude waves without increasing false positives. As shown in Fig. 7, the P wave at time instant 4.45 is well estimated.

Once we have obtained the P and T-wave locations, the corresponding wave amplitudes can be estimated by using (6). Fig. 8 shows the posterior distributions $p\left(\mathbf{a}_k|\mathbf{x}\right)$ and the estimates $\hat{a}_k$ of P-wave amplitudes at time 1.5s, 2.3040s, 3.1520s and 4.4520s. Similarly, the noise variance can be estimated by the MMSE estimator (8). The estimated posterior distribution

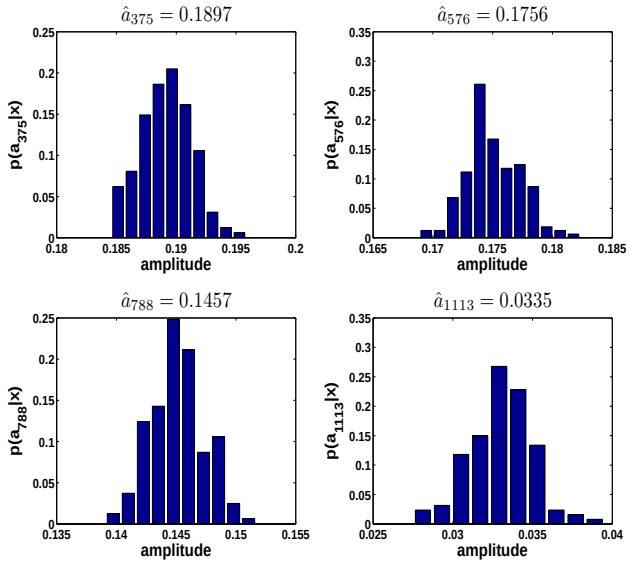


Fig. 8. Posterior distributions of the P-wave amplitudes $p\left(\mathbf{a}_k|\mathbf{x}\right)$ with $k \in \{579, 780, 991, 1322\}$.

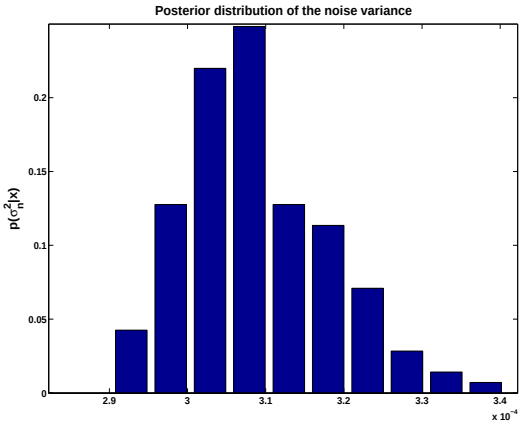


Fig. 9. Posterior distribution of the noise variance $\sigma_n^2$.

of the noise variance $p\left(\sigma_n^2|\mathbf{x}\right)$ is shown in Fig. 9 for this first example.

As presented previously, P and T-wave delineation is based on the estimated waveform coefficients $\hat{\mathbf{h}}$ according to (7). The delineation results of "sele0136" compared with manual annotations of expert are illustrated in Fig. 10 (top), whereas the estimated waveform of P and T-wave for 1 minute signal length are presented in Fig. 10 (left) and Fig. 10 (right).

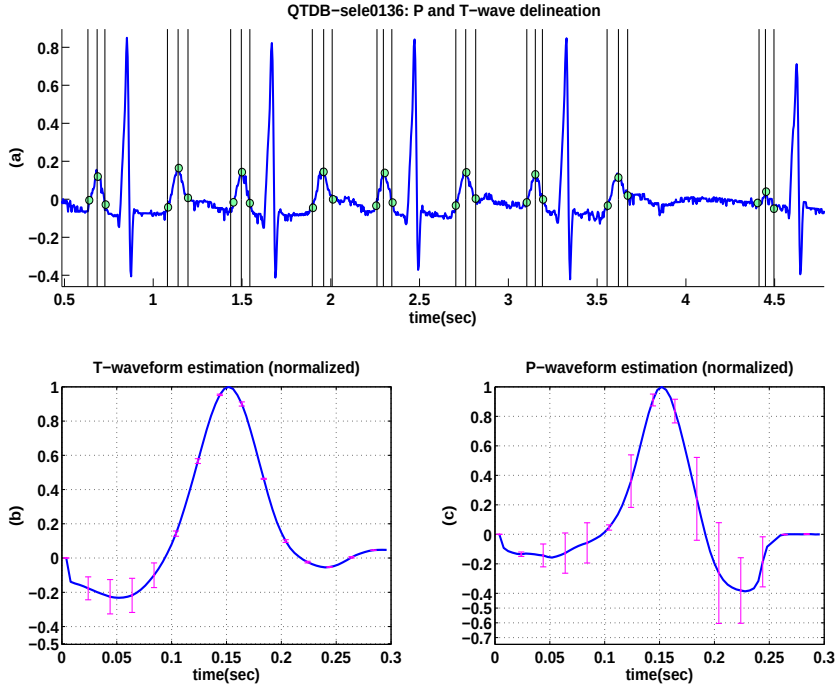


Fig. 10. Results of processing QTDB dataset sele0136, channel 1, start from minute 10. (a) Delineation results: the vertical lines show the manual annotations by expert and the markers show the results of the proposed algorithm. (b) The mean (in blue) and standard deviations (in pink) of estimated T-waveform for 1 minute signal length. (c) The mean (in blue) and standard deviations (in pink) of estimated P-waveform for 1 minute signal length.

### *B. P and T-wave delineation for different wave morphologies*

Since the proposed method estimates the P and T-waveform shapes pointwise for each processing window, it is able to adapt to various wave morphologies. This section shows some other representative results obtained with the proposed method on QTDB. The first example considers the first channel of QTDB referred to as “sel16539”, where both P and T-waves are associated to normal patients. The delineation results for the P and T-waves are shown in Fig. 11.b, whereas the estimated waveform of P and T-wave for each processing block are presented in Fig. 11.c and Fig. 11.d. All kinds of slope, magnitude and polarity for the P and T-waves are successfully detected and delineated for this example. The second example considers feeble P-waves and inverted T-waves by using the first channel of QTDB dataset “sel306”. The results presented in Fig. 12 show that the proposed method allows a good waveform estimation for inverted waves. This is particularly interesting for the observation of wave morphology evolution. Fig. 13 illustrates the delineation result of prominent T-

waves and feeble P-waves by using the first channel of QTDB dataset “sel308” whereas the delineation of noisy feeble P and T-waves is shown in Fig. 14 by using the first channel of QTDB dataset “sele0607”. The delineation results of biphasic T-waves are illustrated in Fig. 15 by using the first channel of QTDB dataset “sel301”. The corresponding delineation results of broad P and T-wave morphology are shown in Fig. 16. All the P and T-waves are successfully detected and well delineated in these examples. Waveform estimations are also very satisfactory. An example of signals that contain premature ventricular contractions (PVCs) is also studied by processing the MIT-BIH dataset “119”. As shown in Fig. 17 and Fig. 18 below, the proposed method can handle these non-monotonic morphological abnormalities. Note in particular that the estimated T-wave of the third beat has been superimposed with the estimated P-wave of the fourth beat, which is in agreement with the presence of a unique wave in the non QRS region. Furthermore, with the help of the proposed signal model, the sudden T-wave amplitude inversion has been detected, which is a nice property for the PVC detection problem.

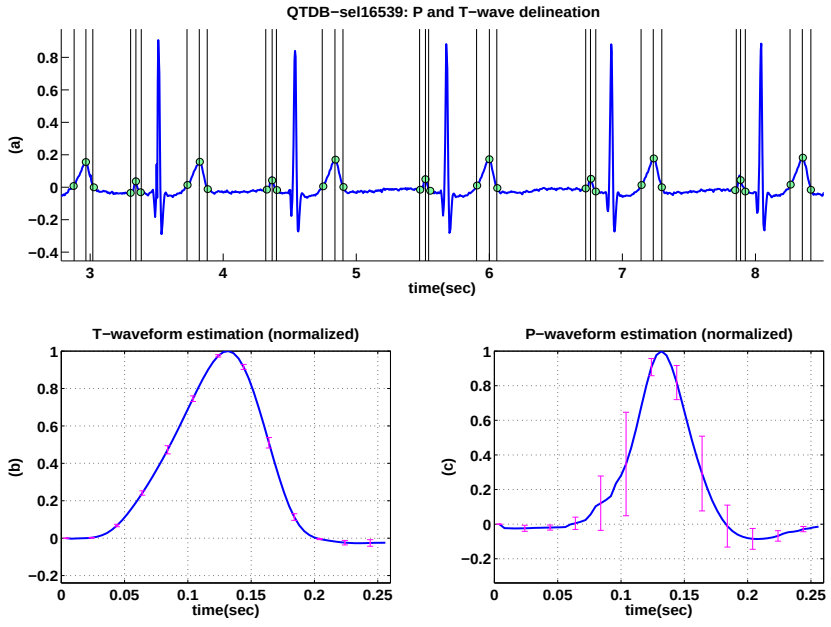


Fig. 11. Results of processing QTDB dataset sel16539, channel 1, start from minute 10. (a) Delineation results: the vertical lines show the manual annotations by expert and the markers show the results of the proposed algorithm. (b) The mean (in blue) and standard deviations (in pink) of estimated T-waveform for 1 minute signal length. (c) The mean (in blue) and standard deviations (in pink) of estimated P-waveform for 1 minute signal length.

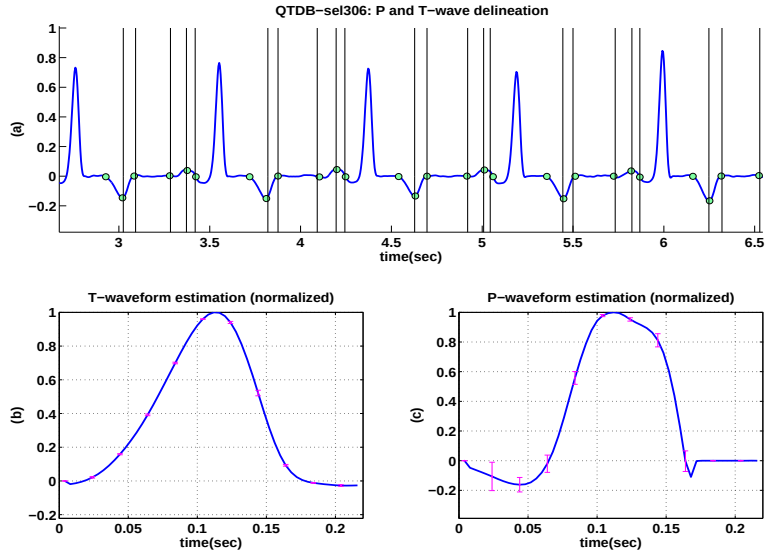


Fig. 12. Results of processing QTDB dataset sel306, channel 1, start from minute 10. (a) Delineation results: the vertical lines show the manual annotations by expert and the markers show the results of the proposed algorithm. Note that the manual annotations for T onset are not available. (b) The mean (in blue) and standard deviations (in pink) of estimated T-waveform for 1 minute signal length. (c) The mean (in blue) and standard deviations (in pink) of estimated P-waveform for 1 minute signal length.

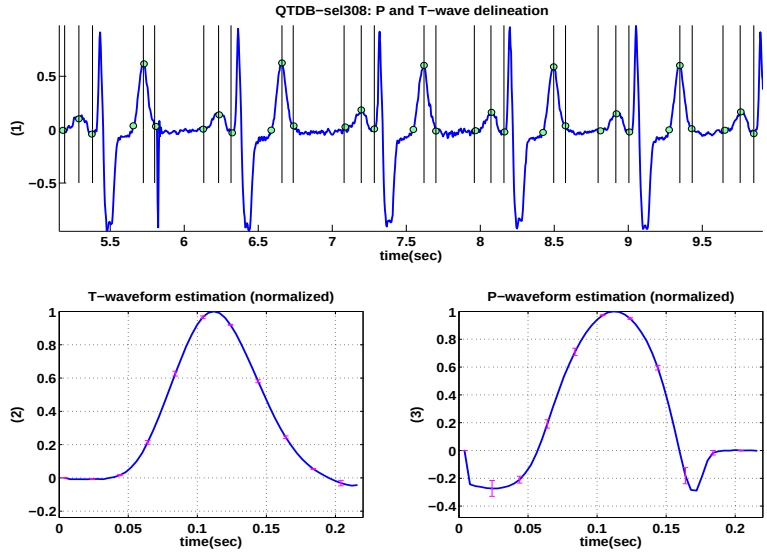


Fig. 13. Results of processing QTDB dataset sel308, channel 1, start from minute 10. (a) Delineation results: the vertical lines show the manual annotations by expert and the markers show the results of the proposed algorithm. Note that the manual annotations for T onset are not available. (b) The mean (in blue) and standard deviations (in pink) of estimated T-waveform for 1 minute signal length. (c) The mean (in blue) and standard deviations (in pink) of estimated P-waveform for 1 minute signal length.

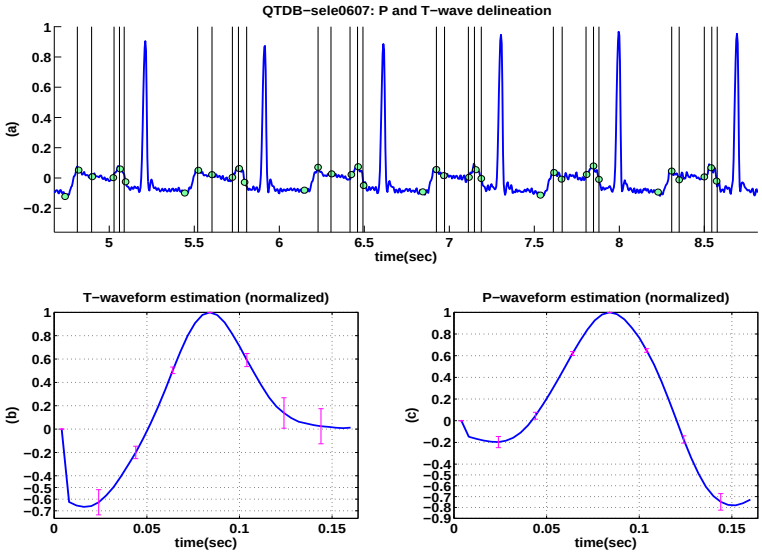


Fig. 14. Results of processing QTDB dataset sel0607, channel 1, start from minute 10. (a) Delineation results: the vertical lines show the manual annotations by expert and the markers show the results of the proposed algorithm. Note that the manual annotations for T onset are not available. (b) The mean (in blue) and standard deviations (in pink) of estimated T-waveform for 1 minute signal length. (c) The mean (in blue) and standard deviations (in pink) of estimated P-waveform for 1 minute signal length.

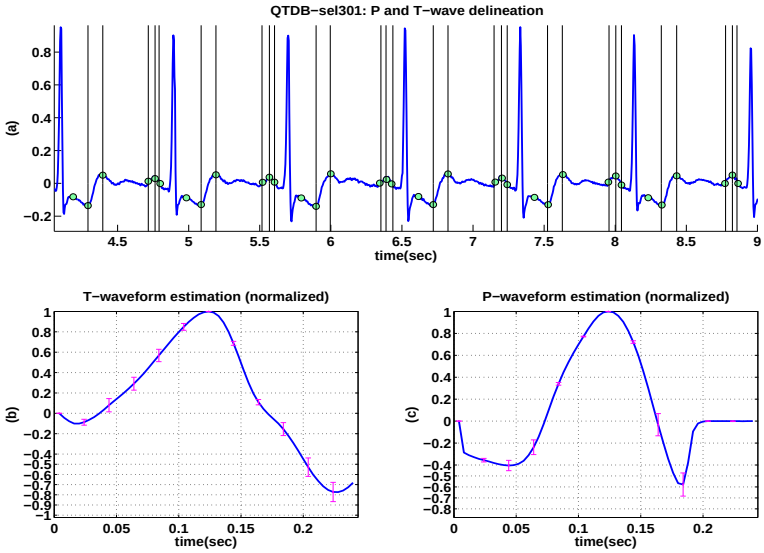


Fig. 15. Results of processing QTDB dataset sel301, channel 1, start from minute 10. (a) Delineation results: the vertical lines show the manual annotations by expert and the markers show the results of the proposed algorithm. Note that the manual annotations for T onset are not available. (b) The mean (in blue) and standard deviations (in pink) of estimated T-waveform for 1 minute signal length. (c) The mean (in blue) and standard deviations (in pink) of estimated P-waveform for 1 minute signal length.

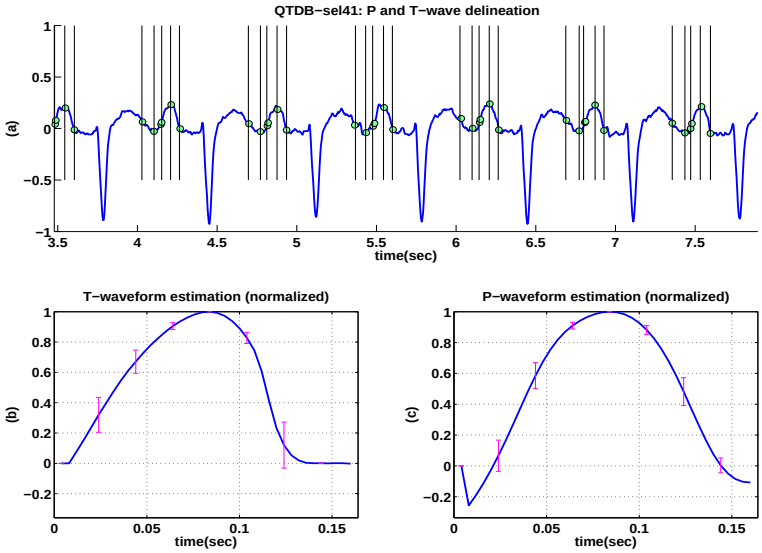


Fig. 16. Results of processing QTDB dataset sel41, channel 1, start from minute 10. (a) Delineation results: the vertical lines show the manual annotations by expert and the markers show the results of the proposed algorithm. (b) The mean (in blue) and standard deviations (in pink) of estimated T-waveform for 1 minute signal length. (c) The mean (in blue) and standard deviations (in pink) of estimated P-waveform for 1 minute signal length.

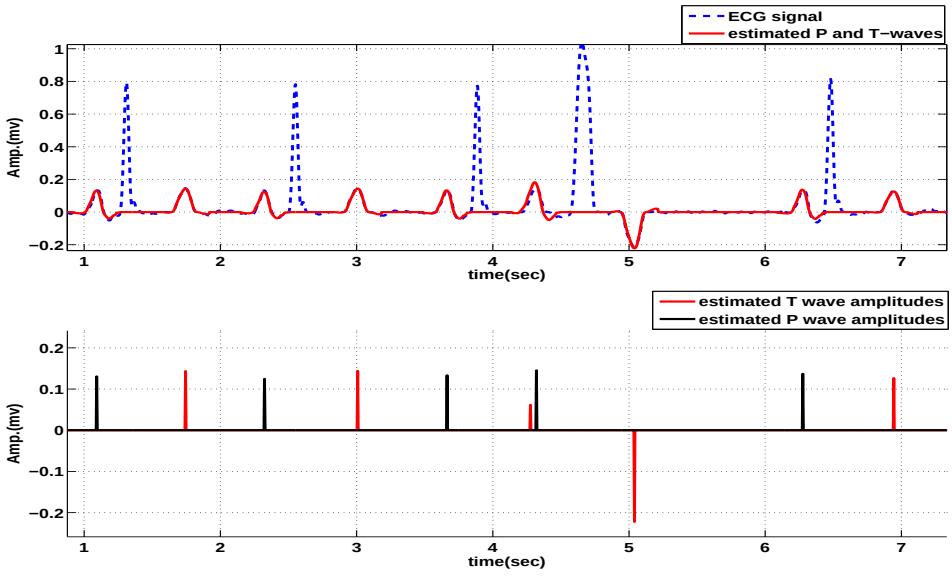


Fig. 17. On the top, preprocessed ECG signal MIT-BIH dataset “119” (dashed blue) and estimated P and T-waves (red). T-waves around the PVC beat (around second 9) are well estimated. On the bottom, the estimated P and T-wave amplitudes for the same signal portion.

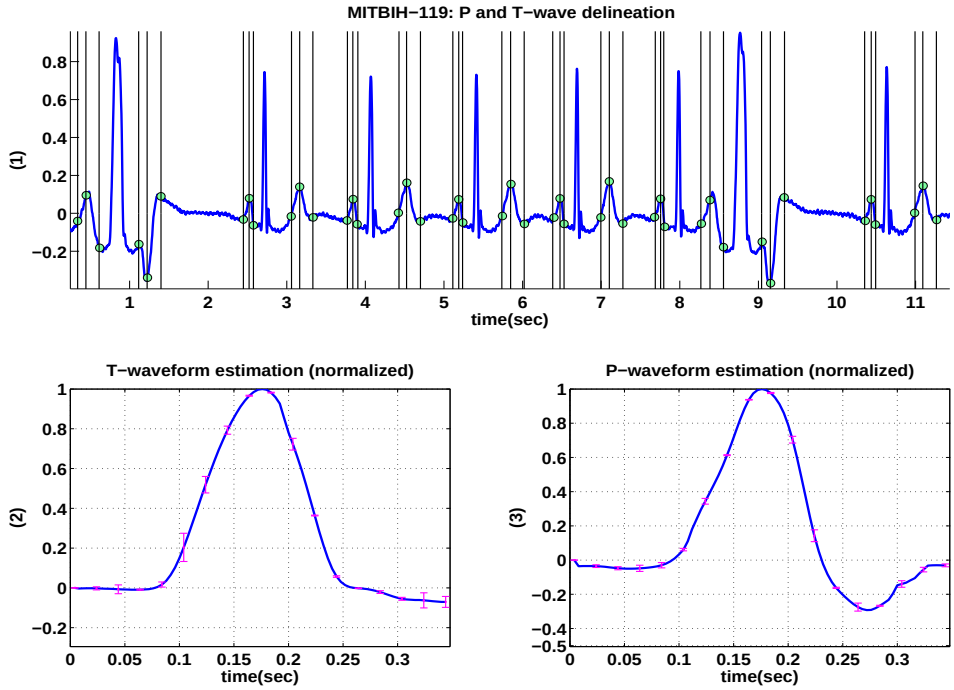


Fig. 18. Results of processing MIT-BIH dataset “119”. (1) Delineation results: the markers show the results of the proposed algorithm. (2) Mean (in blue) and standard deviations (in pink) of the estimated T-waveform for 1 minute of signal length. (3) Mean (in blue) and standard deviations (in pink) of the estimated P-waveform for 1 minute of signal length.

### C. P and T-wave Delineation - Analytical results

The analytical evaluation of the P and T-wave detection can be performed by calculating the sensitivity (also referred to as detection rate) $Se = TP/\left(TP + FN\right)$ and positive predictivity $P^{+} = TP/\left(TP + FP\right)$, where TP denotes the number of true positive detections (wave was present and has been detected), FN stands for the number of false negative detections (wave was present but has been missed) and FP stands for the number of false positive (wave was not present and has been detected). Moreover, the performance of wave delineation is measured by the average of the errors $m$, which stands for the time differences between cardiologist annotations and results of the proposed automatic method. The average of the intra-recording standard deviations denoted as $s$ was also computed. As explained in [7], we consider the absent reference mark on an annotated beat as a no present wave decision, which means that the obtained $P^{+}$ can be interpreted as a lower limit for the actual sensitivity. The analytical validation results obtained with the MCMC-based delineator and the results of three other methods on the QTDB mentioned in [2], [7] and [19] are given in Table I. Despite the relatively small number of $T_{on}$ annotations provided by cardiologists in QTDB, we have still counted the results independently from $T_{\text{peak}}$ and $T_{\text{end}}$. It should also be noted that the proposed algorithm requires an a priori QRS detection. All ECG signals used in this report have been preprocessed by Pan $et\ al.$'s QRS detection algorithm (as presented in Section II), resulting in an overall QRS detection result of $Se = 99.7\%$ and $P^{+} = 99.6\%$. The beats where QRS complexes are not well detected have been excluded from the P and T-wave evaluation.

The detection results on the QTDB show that the proposed method can detect with high sensitivity the P and T-waves annotated by cardiologists in the ECG signals. We obtained a sensitivity of $Se = 98.93\%$ for the P-waves and a sensitivity of $Se = 99.81\%$ for the T-waves, results which are slightly better than the ones obtained with the other methods. As for the positive predictivity, despite it is a pessimiste estimate of the actual $P^{+}$ (which is not possible to calculate), we have still obtained good results since $P^{+} = 97.4\%$ for the P-waves and $P^{+} = 98.97\%$ for the T-waves, which outperforms the other algorithms evaluated in Table I. This is partly because the minimum-distance constraint in Bayesian detection reduces the probability of false positive. The delineation performance is also presented in Table I. The proposed algorithm can delineate the annotated P and T-waves with mean errors $m$ that do not exceed two samples (8 ms). The standard deviations $s$ are around four samples for the

P-wave and five samples for the T-wave, which is quite satisfactory.

TABLE I

DELINEATION AND DETECTION PERFORMANCE COMPARISON IN THE QTDB. (N/A: NOT AVAILABLE)

| Method | Parameters | $P_{\text{on}}$ | $P_{\text{peak}}$ | $P_{\text{end}}$ | $T_{\text{on}}$ | $T_{\text{peak}}$ | $T_{\text{end}}$ |
|---|---|---|---|---|---|---|---|
| PCGS (this work) | annotations | 3176 | 3176 | 3176 | 1345 | 3403 | 3403 |
| | $Se\,(\%)$ | 98.93 | 98.93 | 98.93 | 99.01 | 99.81 | 99.81 |
| | $P^{+}\,(\%)$ | 97.40 | 97.40 | 97.40 | 96.07 | 98.97 | 98.97 |
| | $m \pm s\,(ms)$ | 3.7±17.3 | 4.1±8.6 | -3.1±15.1 | 7.1±18.5 | 1.3±10.5 | 4.3±20.8 |
| WT [7] | annotations | 3194 | 3194 | 3194 | N/A | 3542 | 3542 |
| | $Se\,(\%)$ | 98.87 | 98.87 | 98.75 | N/A | 99.77 | 99.77 |
| | $P^{+}\,(\%)$ | 91.03 | 91.03 | 91.03 | N/A | 97.79 | 97.79 |
| | $m \pm s\,(ms)$ | 2.0±14.8 | 3.6±13.2 | 1.9±12.8 | N/A | 0.2±13.9 | -1.6±18.1 |
| LPD [2] | $Se\,(\%)$ | 97.70 | 97.70 | 97.70 | N/A | 99.00 | 99.00 |
| | $P^{+}\,(\%)$ | 91.17 | 91.17 | 91.17 | N/A | 97.74 | 97.74 |
| | $m \pm s\,(ms)$ | 14.0±13.3 | 4.8±10.6 | -0.1±12.3 | N/A | -7.2±14.3 | 13.5±27.0 |
| Analysis of TU complexes [19] | $Se\,(\%)$ | N/A | N/A | N/A | N/A | 92.60 | 92.60 |
| | $P^{+}\,(\%)$ | N/A | N/A | N/A | N/A | N/A | N/A |
| | $m \pm s\,(ms)$ | N/A | N/A | N/A | N/A | -12.0±23.4 | 0.8±30.3 |

Moreover, the histograms of deviations between the results of the proposed algorithm compared to the "gold standard" of cardiologist manually measured TP interval ($\text{TP}_{\text{int}} = \text{T}_{\text{peak}} - \text{P}_{\text{peak}}$), P wave duration ($\text{P}_{\text{dur}} = \text{P}_{\text{onset}} - \text{P}_{\text{end}}$), ST interval ($\text{ST}_{\text{int}} = \text{S}_{\text{peak}} - \text{T}_{\text{end}}$) and $\text{QT}^{p}$ interval ($\text{QT}^{p}_{\text{int}} = \text{Q}_{\text{peak}} - \text{T}_{\text{peak}}$) are presented in Fig. 19. The deviations of the PCGS based method are similar to the results obtained with recent proposed method [15]. Smaller deviations (mostly below 8 ms) have been obtained for those detections which rely on peak points, i.e., $\text{TP}_{\text{int}}$ and $\text{QT}^{p}_{\text{int}}$. For those detections which rely on peak boundaries, the deviations are also in the acceptable range (mostly below 20 ms). Note that the proposed method focuses on P and T-wave analysis problem, thus the deviations of QRS locations are not considered in the validation.

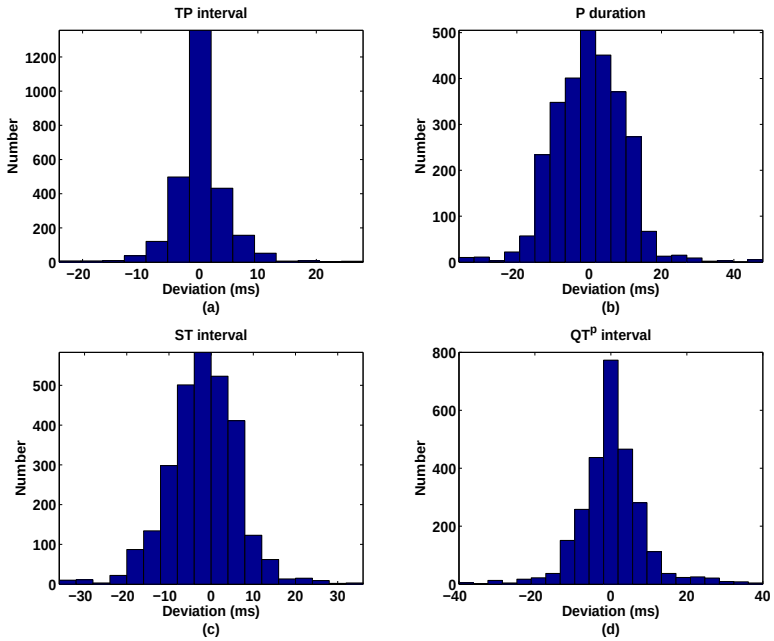


Fig. 19. Histograms of deviations between the markings of the proposed automatic algorithm compared to the "gold standard" of manually measured annotations including (a) TP interval, (b) P wave duration, (c) ST interval and (d) $QT^p$ interval.

### *D. Comparison with a method based on a Gaussian mixture model*

In [15], Sayadi $et\ al.$ have proposed an interesting ECG segmentation approach based on Kalman filters (KF). With the help of O. Sayadi, we have carried out a comparison of the PCGS based method with the KF based method. Some qualitative comparisons of the two methods on several representative datasets from the QT database are presented in Fig. 20-23. It can be seen that the PCGS estimates are closer to the manual annotations (depicted by vertical black lines) than the estimates resulting from [15]. Meanwhile, Fig. 25 shows the absolute errors of $T_{\text{peak}}$, $T_{\text{end}}$, $P_{\text{on}}$, $P_{\text{peak}}$ and $P_{\text{end}}$ for the delineation results of the two methods (the absolute error of a given parameter vector is defined as the norm of the difference between the actual value of the parameter vector and its estimate). These results have been obtained for 118 representative signals from the QT database. It appears that the proposed PCGS provides smaller errors than the KF based method of [15], especially when considering pathological ECG signals (the Gaussian mixture model studied in [15] is more appropriate to normal ECG signals).

To finish, based on the comparison between the two methods, it should also be noted that

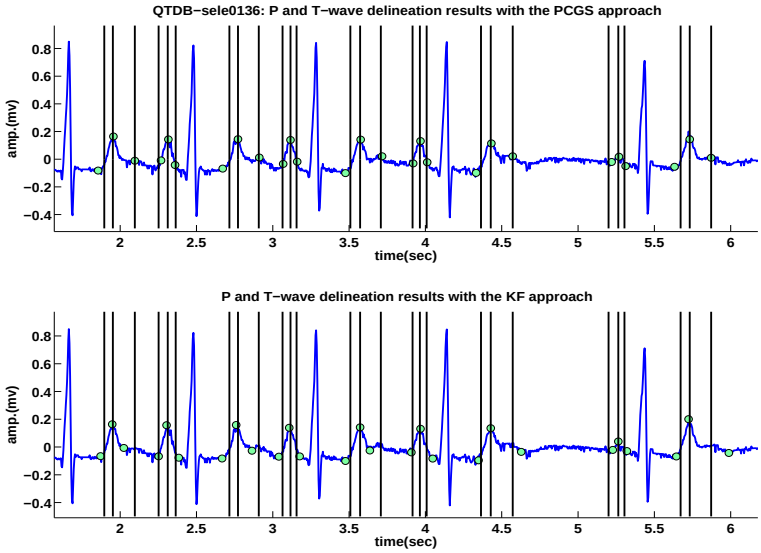


Fig. 20. Delineation results for QT database “sele0136”, which presents some rhythm changes with different amplitudes between P and T-waves. The upper plot shows the results of the proposed PCGS method, and the lower plot shows the results of the method proposed in [15]. The vertical lines in both of two plots show the manual detection results provided by cardiologists.

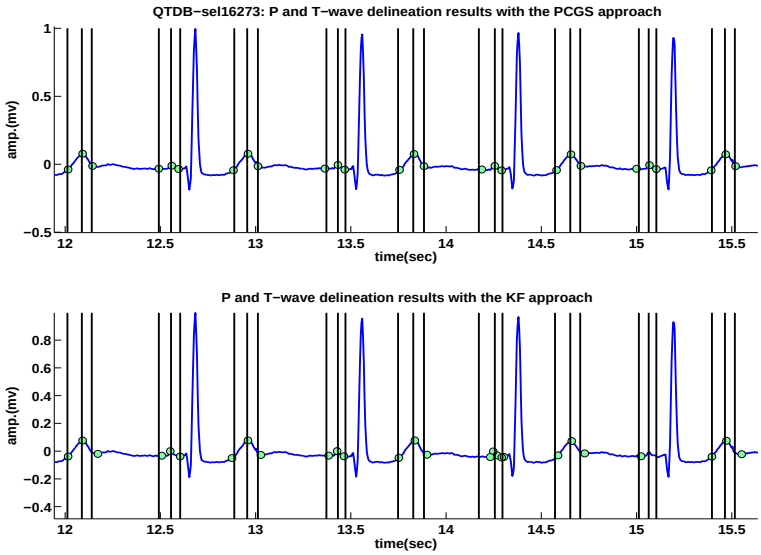


Fig. 21. Delineation results for QT database “sel16273”. The upper plot shows the results of the proposed PCGS method, and the lower plot shows the results of the method proposed in [15]. The vertical lines in both of two plots show the manual detection results provided by cardiologists.

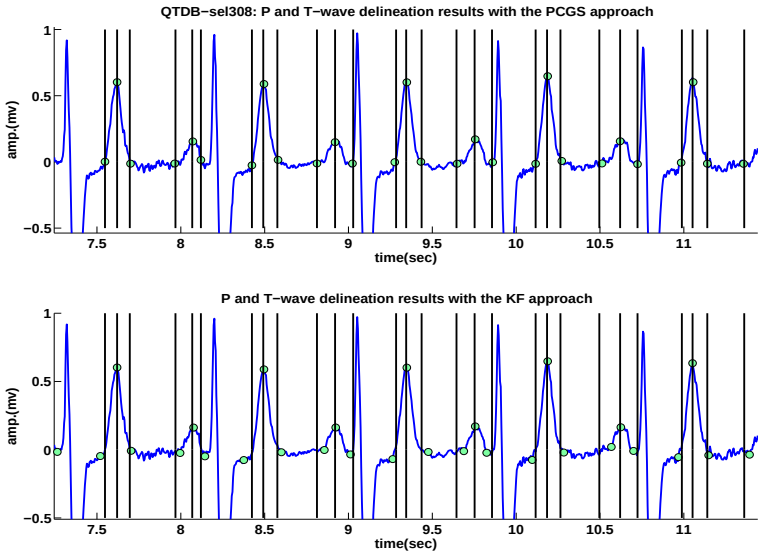


Fig. 22. Delineation results for QT database “sel308”. The upper plot shows the results of the proposed PCGS method, and the lower plot shows the results of the method proposed in [15]. The vertical lines in both of two plots show the manual detection results provided by cardiologists.

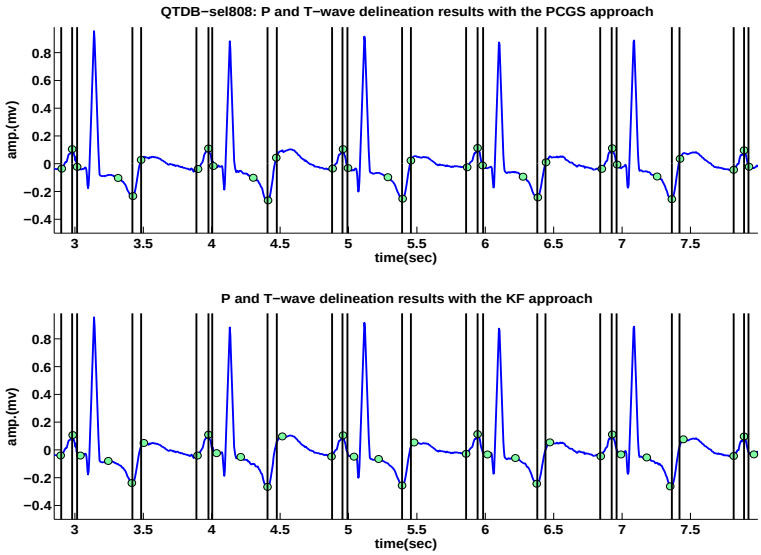


Fig. 23. Delineation results for QT database “sel808”. The upper plot shows the results of the proposed PCGS method, and the lower plot shows the results of the method proposed in [15]. The vertical lines in both of two plots show the manual detection results provided by cardiologists.

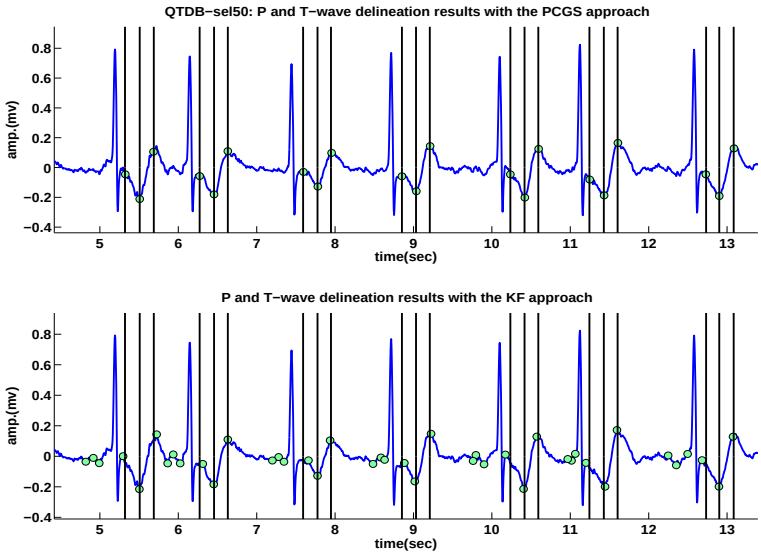


Fig. 24. Delineation results for QT database “sel50”, which is classified as “no P-wave” pathology. The upper plot shows the results of the proposed PCGS method, and the lower plot shows the results of the method proposed in [15]. The vertical lines in both of two plots show the manual detection results provided by cardiologists.

1) the performance of the KF method depends on its initialization which can be difficult to adjust, 2) the Gaussian mixture model and the KF method of [15] are not really appropriate to ECG signals with abnormal rhythms contrary to the PCGS that estimates the whole P and T wave shapes (since the KF method always determines a fixed number of Gaussian kernels to fit the data). Moreover, the algorithm of [15] is not able to handle the absence of T or P-wave in some pathological ECGs, contrary to the PCGS method. As shown in Fig. 24, the KF method detect P-waves in dataset “sel50” from the QT database (see green circles before the QRS) while the cardiologists have classified all signals from this dataset as “no P-wave” pathologies. Conversely, the PCGS method does not detect the P waves for these signals, as desired. The price to pay with the good perfomance of the proposed PCGS is its computational complexity which is significantly larger than the KF method of [15].

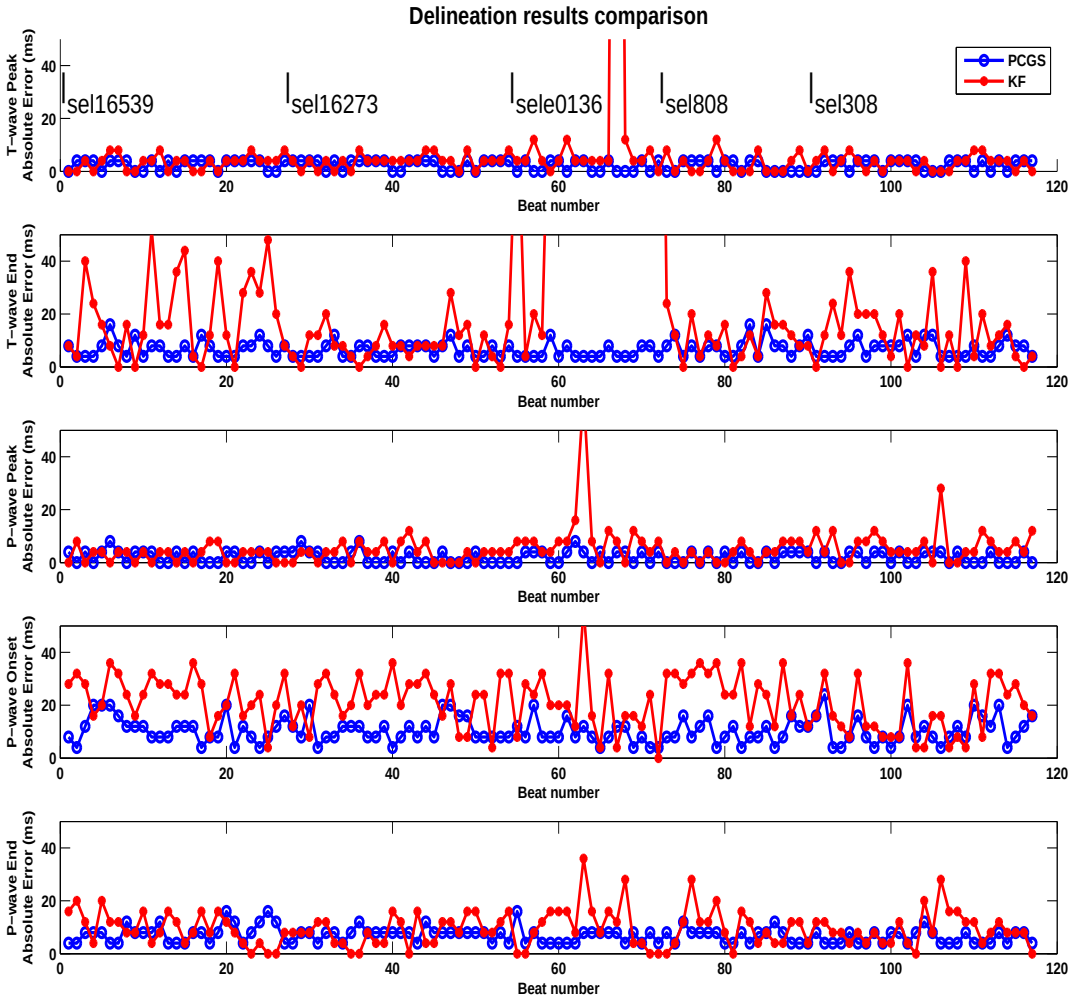


Fig. 25. Absolute errors between the estimated values of $T_{\text{peak}}$, $T_{\text{end}}$, $P_{\text{on}}$, $P_{\text{peak}}$ and $P_{\text{end}}$ and manual annotations for representative signals from the QT datasets “sel16539”, “sel16273”, “sele0136”, “sel808” and “sel308” (blue empty circles correspond to the PCGS method whereas red full circles correspond to the results provided by O. Sayadi associated to the method of [15].

### *E. Receiver operating characteristics for P and T-wave detection*

Receiver operating characteristics (ROC) have been performed to select possibly optimal values of $\gamma_P$ and $\gamma_T$. The ROC curve for P-wave detection has been computed using three typical datasets and three "no P-wave" datasets available in QT database. The results depicted in Fig. 26(a) show the good performance of the proposed detector. Of course, the threshold $\gamma_P$ can be determined from a fixed probability of false alarm (PFA) using this ROC. For the QT database, we have chosen a threshold $\gamma_P = 0.4$ corresponding to a probability of detection PD=1 and PFA=0.05. Similarly, the ROC curve for T-wave can be calculated based on three typical datasets from the QT database and three synthesized "no T-wave" datasets (since the QT database does not contain signals classified as "no T-wave"). A good detection performance can also be confirmed as shown in Fig. 26(b). For the QT database, we have chosen $\gamma_T = 0.55$ that corresponds to PD=1 and PFA =0.01.

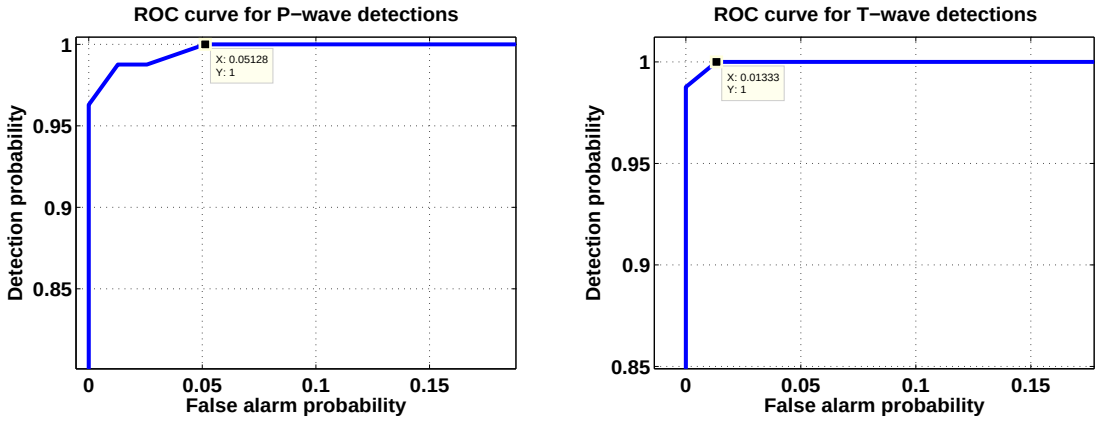


(a) ROC curve for P-wave detection

(b) ROC curve for T-wave detection

Fig. 26. ROC analysis for P and T-wave detection.

### *F. Convergence diagnostic*

A crucial issue when using MCMC methods is convergence assessment, which can help us to determine appropriate values of the numbers of burn-in iterations $N_{\text{bi}}$ and computation iterations $N_r$. To monitor the convergence of the proposed MCMC approach, we have implemented the multivariate potential scale reduction factor (MPSRF) criterion proposed by Brooks $et\ al.$ in [34]. This diagnostic is based on the comparison between estimates resulting from $p$ parallel Monte Carlo chains as follows

$$\text{MPSRF} = \frac{p-1}{p} + \frac{q+1}{q}\text{eig}\left(\mathbf{V}_{\text{intra}}^{-1}\mathbf{V}_{\text{inter}}\right) \tag{10}$$

where the inter-chain and intra-chain covariance matrices are defined as follows

$$\mathbf{V}_{\text{intra}} = \frac{1}{p\,(q-1)} \sum_{j=1}^{p} \sum_{t=1}^{q} \left(\psi_{jt} - \overline{\psi}_{j\cdot}\right) \left(\psi_{jt} - \overline{\psi}_{j\cdot}\right)^{T} \tag{11}$$

$$\mathbf{V}_{\text{inter}} = \frac{1}{p-1} \sum_{j=1}^{p} \left(\psi_{j\cdot} - \overline{\psi}_{\cdot\cdot}\right) \left(\psi_{j\cdot} - \overline{\psi}_{\cdot\cdot}\right)^{T} \tag{12}$$

and where $\left\{\psi_{jt}^{(i)}, j = 1, \ldots, p; t = 1, \ldots, q\right\}$ denotes the $i$th element of the parameter vector $\psi$ in chain $j$ at time $t$, $\overline{\psi}_{j\cdot}$ (respectively $\overline{\psi}_{\cdot\cdot}$) denotes the local mean (respectively global mean) of chains and $\text{eig}\,(\mathbf{V})$ is the largest eigenvalue of the positive-definite matrix $\mathbf{V}$.

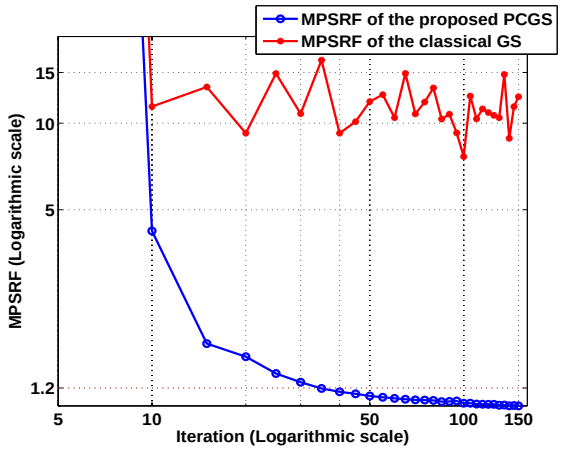


Fig. 27. Evolution of MPSRF criterion on QTDB dataset "sele0136" for the unknown parameters ($\psi = \left(\hat{\mathbf{b}}, \hat{\mathbf{a}}, \hat{\mathbf{h}}\right)$), the proposed PCGS in blue and the classical GS in red.

As an example, Fig. 27 shows the MPSRF criterion applied on signals from QTDB dataset "sele0136" on $p = 10$ independent chains of the proposed PCGS and the classical GS for $\psi = \left(\hat{\mathbf{b}}, \hat{\mathbf{a}}, \hat{\mathbf{h}}\right)$. Since a value of MPSRF below 1.2 is recommended in [34], the criterion confirms a good convergence of the proposed sampler with $N_{\text{bi}} = 40$ burn-in iterations, which outperforms significantly the classical GS.

## VI. Conclusions and Future Works

This report studied a Bayesian sampling algorithm performing joint P and T-wave delineation and waveform estimation. Instead of deploying rigid detection and delineation criteria for all ECG time series, we used a local detection strategy and a flexible delineation criteria based on the estimation of P and T waveforms in consecutive beat-processing windows. The proposed algorithm can be summarized as follows

- Preprocessing: QRS detection, baseline removal and definition of search windows
- Generation of samples asymptotically distributed according to the posterior distribution using a PCGS
- Estimation of the P and T-wave peak locations, amplitudes and waveform coefficients based on the generated samples using MMSE estimators
- P and T-wave detection and delineation based on the estimated P and T-wave peak locations, amplitudes and waveform coefficients

The main contributions of this work are: 1) The introduction of a hierarchical Bayesian model for P and T-wave delineation. This model is based on a modified Bernoulli-Gaussian sequence with minimum distance constraint for the wave locations and amplitudes and appropriate priors for the wave impulse responses and noise variance. 2) The derivation of a PCGS allowing one to generate samples distributed according to the posterior distribution associated to the previous hierarchical Bayesian model. The proposed PCGS overcomes the slow convergence problem which the classical Gibbs sampler exhibits when processing parameters with strong local dependencies. To our knowledge, it is the first time this kind of simulation method is applied to ECG segmentation problems. 3) The proposed method allows us to estimate simultaneously the P and T-wave fiducial points and the P and T-waveforms, which is rarely done by other ECG delineation methods. 4) The PCGS based method allows us to determine the confidence intervals which provide the reliability information of the estimates. This could also be useful for medical diagnosis.

The resulting algorithm was validated using the entire annotated QT database. A comparison with other benchmark methods showed that the proposed method provides a reliable detection and an accurate delineation for a wide variety of wave morphologies. The most significant improvement was found in the P and T-wave detection rate and the positive predictivity. In addition, the proposed method can also provide waveform estimation. We have to mention here that the price to pay with the proposed algorithm is a higher computational cost when compared to other more classical methods.

It is also interesting to note that our algorithm also allows observation of the waveform evolution among processing blocks. If we extract T-wave search region on every-other-beat rather than successively, the proposed method can be directly used to perform TWA analysis. Indeed, the wave amplitude can be used to decide the presence or absence of TWA, while the waveform estimation can reflect the characterization of TWA waveform. This study is currently under investigation.

# APPENDIX

## PROOF OF THE SAMPLING DISTRIBUTIONS

**Indicators.** The sampling distribution for $\mathbf{b}_{J_d(k)}$ can be obtained as follows

$$\begin{aligned}
&p\left(\mathbf{b}_{J_d(k)}|\mathbf{b}_{\sim J_d(k)},\mathbf{a}_{\sim J_d(k)},\mathbf{h},\sigma_n^2,\mathbf{x}\right)\\
&\quad\propto p\left(\mathbf{b}_{J_d(k)},\mathbf{b}_{\sim J_d(k)},\mathbf{a}_{\sim J_d(k)},\mathbf{h},\sigma_n^2,\mathbf{x}\right)\\
&\quad\propto p\left(\mathbf{x}|\mathbf{b},\mathbf{a}_{\sim J_d(k)},\mathbf{h},\sigma_n^2\right)p\left(\mathbf{a}|\mathbf{b}\right)p\left(\mathbf{b}\right)p\left(\mathbf{h}\right)p\left(\sigma_n^2\right)\\
&\quad\propto p\left(\mathbf{x}|\mathbf{b},\mathbf{a}_{\sim J_d(k)},\mathbf{h},\sigma_n^2\right)p\left(\mathbf{a}|\mathbf{b}\right)p\left(\mathbf{b}\right)\\
&\quad\propto\left[\int p\left(\mathbf{x}|\mathbf{b},\mathbf{a},\mathbf{h},\sigma_n^2\right)p\left(\mathbf{a}_{J_d(k)}|\mathbf{b}_{J_d(k)}\right)\mathrm{d}\mathbf{a}_{J_d(k)}\right]p\left(\mathbf{b}\right)
\end{aligned}$$

Using the minimum-distance constraint, there can only be one non-zero wave indicator within the neighborhood $J_{d(k)}$. Let $k^{'}\in J_{d(k)}$ denote this only non-zero indicator location, $\mathbf{b}_{J_d(k)}$ can be seen as two parts

$$\begin{cases} b_{k'}=1\\ b_m=0, m\in J_d\left(k\right)\setminus k^{'}\end{cases}$$

where $J_d\left(k\right)\setminus k^{'}$ denotes the set of locations within the neighborhood $J_{d(k)}$ excluding $k^{'}$. The conditional distribution can be further developped by inserting all the prior distributions

$$\begin{aligned}
&p\left(\mathbf{b}_{J_d(k)}|\mathbf{b}_{\sim J_d(k)},\mathbf{a}_{\sim J_d(k)},\mathbf{h},\sigma_n^2,\mathbf{x}\right)\\
&\quad\propto\int\exp\left[-\frac{1}{2\sigma_n^2}\left\|\underbrace{\mathbf{x}-\mathbf{F}_{\sim J_d(k)}\mathbf{B}_{\sim J_d(k)}\mathbf{a}_{\sim J_d(k)}}_{\tilde{\mathbf{x}}}\right.\right.\\
&\qquad\left.\left.-\mathbf{F}_{J_d(k)}\mathbf{B}_{J_d(k)}\mathbf{a}_{J_d(k)}\right\|^2-\frac{a_{k'}}{2\sigma_a^2}\right]\prod_{m\in J_d(k)\setminus k'}\delta\left(a_m\right)\mathrm{d}\mathbf{a}_{J_d(k)}p\left(\mathbf{b}\right)\\
&\quad\propto\left[\int\exp\left[-\frac{1}{2\sigma_n^2}\left\|\tilde{\mathbf{x}}-f_{k'}a_{k'}\right\|^2-\frac{a_{k'}}{2\sigma_a^2}\right]\mathrm{d}a_{k'}\right]p\left(\mathbf{b}\right)\\
&\quad\propto\left[\int\exp\left[-\frac{1}{2}\left(a_{k'}\underbrace{\left(\frac{f_{k'}^Tf_{k'}}{\sigma_n^2}+\frac{1}{\sigma_a^2}\right)}_{\frac{1}{\sigma_1^2}}a_{k'}-a_{k'}\underbrace{\frac{f_{k'}^T\tilde{\mathbf{x}}}{\sigma_n^2}}_{\frac{\mu_1}{\sigma_1^2}}-\frac{\tilde{\mathbf{x}}^Tf_{k'}}{\sigma_n^2}a_{k'}\right)\right]\mathrm{d}a_{k'}\right]p\left(\mathbf{b}\right)\\
&\quad\propto\left[\int\exp\left[-\frac{\left(a_{k'}-\mu_1\right)^2}{2\sigma_1^2}+\frac{\mu_1^2}{2\sigma_1^2}\right]\mathrm{d}a_{k'}\right]p\left(\mathbf{b}\right)\\
&\quad\propto\sigma_1\exp\left[\frac{\mu_1^2}{2\sigma_1^2}\right]p\left(\mathbf{b}\right)
\end{aligned}$$

where $\sigma_1^2$ and $\mu_1$ contain information about $\mathbf{b}_{J_d(k)}$ and are defined as

$$\begin{aligned}\sigma_1^2 &= \left(\frac{\|f_{k'}\|^2}{\sigma_n^2}+\frac{1}{\sigma_a^2}\right)^{-1} = \left(\frac{\left\|\mathbf{F}_{J_d(k)}\mathbf{b}_{J_d(k)}\right\|^2}{\sigma_n^2}+\frac{1}{\sigma_a^2}\right)^{-1}\\ \mu_1 &= \frac{\sigma_1^2 f_{k'}^T\tilde{\mathbf{x}}}{\sigma_n^2} = \frac{\sigma_1^2\mathbf{b}_{J_d(k)}^T\mathbf{F}_{J_d(k)}^T\tilde{\mathbf{x}}}{\sigma_n^2}.\end{aligned}$$

**Amplitudes.** The sampling distribution for $a_k$ can be obtained as follows

$$\begin{aligned}&p\left(a_k|b_k=1,\mathbf{b}_{\sim J_d(k)},\mathbf{a}_{\sim J_d(k)},\mathbf{h},\sigma_n^2,\mathbf{x}\right)\\ &\quad\propto\int p\left(\mathbf{a}_{J_d(k)}|\mathbf{b},\mathbf{a}_{\sim J_d(k)},\mathbf{h},\sigma_n^2,\mathbf{x}\right)\mathrm{d}\mathbf{a}_{J_d(k)\backslash k}\\ &\quad\propto\int p\left(\mathbf{x}|\mathbf{b},\mathbf{a},\mathbf{h},\sigma_n^2\right)p\left(\mathbf{a}_{J_d(k)}|\mathbf{b}_{J_d(k)}\right)\mathrm{d}\mathbf{a}_{J_d(k)\backslash k}\end{aligned}$$

Consequently, similar to the conditional distribution of $\mathbf{b}_{J_d(k)}$, the following results can be obtained

$$\begin{aligned}&p\left(a_k|b_k=1,\mathbf{b}_{\sim J_d(k)},\mathbf{a}_{\sim J_d(k)},\mathbf{h},\sigma_n^2,\mathbf{x}\right)\\ &\quad\propto\int\exp\left[-\frac{1}{2\sigma_n^2}\left\|\tilde{\mathbf{x}}-\mathbf{F}_{J_d(k)}\mathbf{B}_{J_d(k)}\mathbf{a}_{J_d(k)}\right\|^2+\frac{a_k}{2\sigma_a^2}\right]\prod_{m\in J_d(k)\backslash k}\delta\left(a_m\right)\mathrm{d}\mathbf{a}_{J_d(k)\backslash k}\\ &\quad\propto\exp\left[-\frac{1}{2\sigma_n^2}\left\|\tilde{\mathbf{x}}-f_k a_k\right\|^2+\frac{a_k}{2\sigma_a^2}\right]\\ &\quad\propto\exp\left[-\frac{1}{2\sigma_1^2}\left(a_k-\mu_1\right)^2\right]\end{aligned}$$

that can be summarized as

$$p\left(a_k|b_k=1,\mathbf{b}_{\sim J_d(k)},\mathbf{a}_{\sim J_d(k)},\mathbf{h},\sigma_n^2,\mathbf{x}\right)=\mathcal{N}\left(\mu_1,\sigma_1^2\right).$$

**Waveform coefficients.** The sampling distribution for **h** can be obtained as follows

$$\begin{aligned}p\left(\mathbf{h}|\mathbf{b},\mathbf{a},\sigma_n^2,\mathbf{x}\right)&\propto p\left(\mathbf{x}|\mathbf{b},\mathbf{a},\mathbf{h},\sigma_n^2\right)p\left(\mathbf{h}\right)\\ &\propto\exp\left[-\frac{1}{2\sigma_n^2}\left\|\mathbf{x}-\mathbf{U}\mathbf{h}\right\|^2\right]\exp\left[-\frac{1}{2\sigma_h^2}\left\|\mathbf{h}\right\|^2\right]\\ &\propto\exp\left[-\frac{1}{2\sigma_n^2}\left[\left\|\mathbf{U}\mathbf{h}\right\|^2-2\mathbf{x}\mathbf{U}\mathbf{h}\right]\right]\exp\left[-\frac{1}{2\sigma_h^2}\left\|\mathbf{h}\right\|^2\right]\\ &\propto\exp\left[-\frac{1}{2}\left(\frac{1}{\sigma_n^2}\left\|\mathbf{U}\right\|^2+\frac{1}{\sigma_h^2}\right)\left\|\mathbf{h}\right\|^2+\frac{1}{\sigma_n^2}\mathbf{x}\mathbf{U}\mathbf{h}\right]\end{aligned}$$

Equivalently,

$$p\left(\mathbf{h}|\mathbf{b},\mathbf{a},\sigma_n^2,\mathbf{x}\right)=\mathcal{N}\left(\boldsymbol{\mu}_2,\boldsymbol{\sigma}_2^2\right)$$

with

$$\boldsymbol{\mu}_2 = \frac{\boldsymbol{\sigma}_2^2 \mathbf{U}^T \mathbf{x}}{\sigma_n^2}, \quad \boldsymbol{\sigma}_2^2 = \left( \frac{\mathbf{U}^T \mathbf{U}}{\sigma_n^2} + \frac{\mathbf{I}_{L+1}}{\sigma_h^2} \right)^{-1}.$$

## REFERENCES


[1] N. V. Thakor and Y. S. Zhu, "Application of adaptive filtering to ECG analysis: Noise cancellation and arrhythmia detection," *IEEE Trans. Biomed. Eng.*, vol. 38, no. 8, pp. 785–793, 1991.

[2] P. Laguna, R. Jané, and P. Caminal, "Automatic detection of wave boundaries in multilead ECG signals: Validation with the CSE database," *Comput. Biomed. Res.*, vol. 27, no. 1, pp. 45–60, 1994.

[3] P. Strumillo, "Nested median filtering for detecting T-wave offset in ECGs," *Electronics Letters*, vol. 38, no. 14, pp. 682–683, 2002.

[4] I. S. N. Murthy and U. C. Niranjan, "Component wave delineation of ECG by filtering in the fourier domain," *Med. & Bio. Eng. Comput.*, vol. 30, pp. 169–176, 1992.

[5] I. S. N. Murthy and G. S. S. D. Prasad, "Analysis of ECG from pole-zero models," *IEEE Trans. Biomed. Eng.*, vol. 39, no. 7, pp. 741–751, 1992.

[6] C. Li, C. Zheng, and C. Tai, "Detection of ECG characteristic points using wavelet transforms," *IEEE Trans. Biomed. Eng.*, vol. 42, no. 1, pp. 21–28, 1995.

[7] J. P. Martínez, R. Almeida, S. Olmos, A. P. Rocha, and P. Laguna, "A Wavelet-based ECG delineator: Evaluation on standard databases," *IEEE Trans. Biomed. Eng.*, vol. 51, no. 4, pp. 570–581, 2004.

[8] A. A. R. Bsoul, S.-Y. Ji, K. Ward, and K. Najarian, "Detection of P, QRS, and T components of ECG using wavelet transformation," in *Proc. of Int. Conf. on Complex Medical Engineering*, vol. 9, no. 11, 2009, pp. 1–6.

[9] S. S. Mehta, S. C. Saxena, and H. K. Verma, "Recognition of P and T waves in electrocardiograms using fuzzy theory," in *Proc. of the First Regional Conference, IEEE Eng. in Med. and Bio. Society*, New Delhi, India, Feb. 1995, pp. 2/54–2/55.

[10] E. D. A. Botter, C. L. Nascimento, and T. Yoneyama, "A neural network with asymmetric basis functions for feature extraction of ECG P waves," *IEEE Trans. on Neural Networks*, vol. 12, no. 5, pp. 1252–1255, 2001.

[11] P. Trahanias and E. Skordalakis, "Syntactic pattern recognition of the ECG," *IEEE Trans. Pattern. Anal. Mach. Intell.*, no. 7, pp. 648–657, 1990.

[12] J. Thomas, C. Rose, and F. Charpillet, "A multi-HMM approach to ECG segmentation," in *Proc. of 18th IEEE Int. Conf. on Tools with Art. Intel.*, Arlington, VA, Nov. 2006, pp. 609–616.

[13] G. D. Clifford and M. Villarroel, "Model-based determination of QT intervals," in *Proc. of Comput. in Cardiol.*, vol. 33, Valencia, Spain, Sept. 2006, pp. 357–360.

[14] O. Sayadi and M. B. Shamsollahi, "Model-based ECG fiducial points extraction using a modified extended Kalman filter structure," in *Proc. of the First Int. Symp. on App. Sc. in Biomed. and Commun. Tech. (ISABEL)*, Aalborg, Denmark, Oct. 2008, pp. 1–5.

[15] ——, "A model-based Bayesian framework for ECG beat segmentation," *J. of Physiol. Measurement*, vol. 30, pp. 335–352, 2009.

[16] F. Gritzali and F. Gehed, "Detection of the P and T waves in an ECG," *Comput. and Biomed. Res.*, vol. 22, pp. 83–91, 1989.

[17] V. S. Chouhan and S. S. Mehta, “Threshold-based detection of P and T-wave in ECG using new feature signal,” *Int. J. of Comp. Science and Net. Security*, vol. 8, no. 2, pp. 144–152, 2008.

[18] Z. Yang, L. Li, and J. Ling, “Approach to recognition of ECG P waves based on approximating functions,” *J. Biomed. Eng.*, vol. 15, no. 2, pp. 120–122, 1998.

[19] J. A. Vila, Y. Gang, J. Presedo, M. Delgado, S. Barro, and M. Malik, “A new approach for TU complex characterization,” *IEEE Trans. Biomed. Eng.*, vol. 47, no. 6, pp. 746–772, 2000.

[20] Z. Elghazzawi and F. Gehed, “A knowledge-based system for arrhythmia detection,” in *Proc. of Comput. in Cardiol.*, Indianapolis, IN, Sept. 1996, pp. 541–544.

[21] J. P. Martínez and S. Olmos, “Methodological principles of T Wave Alternans analysis: A unified framework,” *IEEE Trans. Biomed. Eng.*, vol. 52, no. 4, pp. 599–613, 2004.

[22] S. M. Narayan and J. M. Smith, “Differing rate dependence and temporal distribution of repolarization alternans in patients with and without ventricular tachycardia,” *J. Cardiovasc. Electrophysiol.*, vol. 10, pp. 61–77, 1999.

[23] C. P. Robert and G. Casella, *Monte Carlo Statistical Methods*. New York: Springer, 2004.

[24] D. A. Van Dyk and T. Park, “Partially collapsed Gibbs samplers: Theory and methods,” *J. Acoust. Soc. Amer.*, vol. 103, pp. 790–796, 2008.

[25] D. Ge, “Décomposition impulsionnelle multi-source. Application aux signaux électromyographiques,” Ph.D. dissertation, École Centrale de Nantes, France, Dec. 2009.

[26] G. Kail, C. Novak, B. Hofer, and F. Hlawatsch, “A blind Monte Carlo detection-estimation method for optical coherence tomography,” in *Proc. IEEE Int. Conf. Acoust., Speech, and Signal Processing (ICASSP)*, Taipei, Taiwan, April 2009, pp. 493–496.

[27] G. Kail, J.-Y. Tourneret, F. Hlawatsch, and N. Dobigeon, “A partially collapsed gibbs sampler for parameters with local constraints,” in *Proc. IEEE Int. Conf. Acoust., Speech, and Signal Processing (ICASSP)*, Dallas, USA, March 2010, pp. 3886–3889.

[28] P. Laguna, R. Mark, A. Goldberger, and G. Moody, “A database for evaluation of algorithms for measurement of QT and other waveform intervals in the ECG,” *Computers in Cardiology*, vol. 24, pp. 673–676, 1997.

[29] J. Pan and W. J. Tompkins, “A real-time QRS detection algorithm,” *IEEE Trans. Biomed. Eng.*, vol. 32, no. 3, pp. 230–236, 1985.

[30] V. S. Chouhan and S. S. Mehta, “Total removal of baseline drift from ECG signal,” in *Proc. of the Int. Conf. on Computing: Theory and Applications*, Kolkata, March 2007, pp. 512–515.

[31] N. Dobigeon, J.-Y. Tourneret, and M. Davy, “Joint segmentation of piecewise constant autoregressive processes by using a hierarchical model and a Bayesian sampling approach,” *IEEE Trans. Signal Process*, vol. 55, pp. 1251–1263, April 2007.

[32] D. Ge, E. L. Carpentier, and D. Farina, “Unsupervised Bayesian decomposition of multi-unit EMG recordings using Tabu search,” *IEEE Trans. Biomed. Eng.*, vol. 56, no. 12, pp. 1–9, Dec. 2009.

[33] H. L. Van Trees, *Detection, Estimation and Modulation Theory*. New York: John Wiley & Sons Inc., 1968.

[34] S. P. Brooks and A. Gelman, “General methods for monitoring convergence of iterative simulations,” *J. of Comput. Graph. Stat.*, vol. 7, no. 4, pp. 434–455, 1998.